Corso di Laurea Magistrale in Ingegneria Elettronica

Fully Biodegradable Temperature Sensors with High Mechanical Stability and Low Thermal Mass

Author:

Filippo Dalla Valle

Superivsors:

Dr. Giovanni Antonio Salvatore
Prof. Gaudenzio Meneghesso
Prof. Andrea Cester

ETH

Eidgenössische Technische Hochschule Zürich
Swiss Federal Institute of Technology Zurich
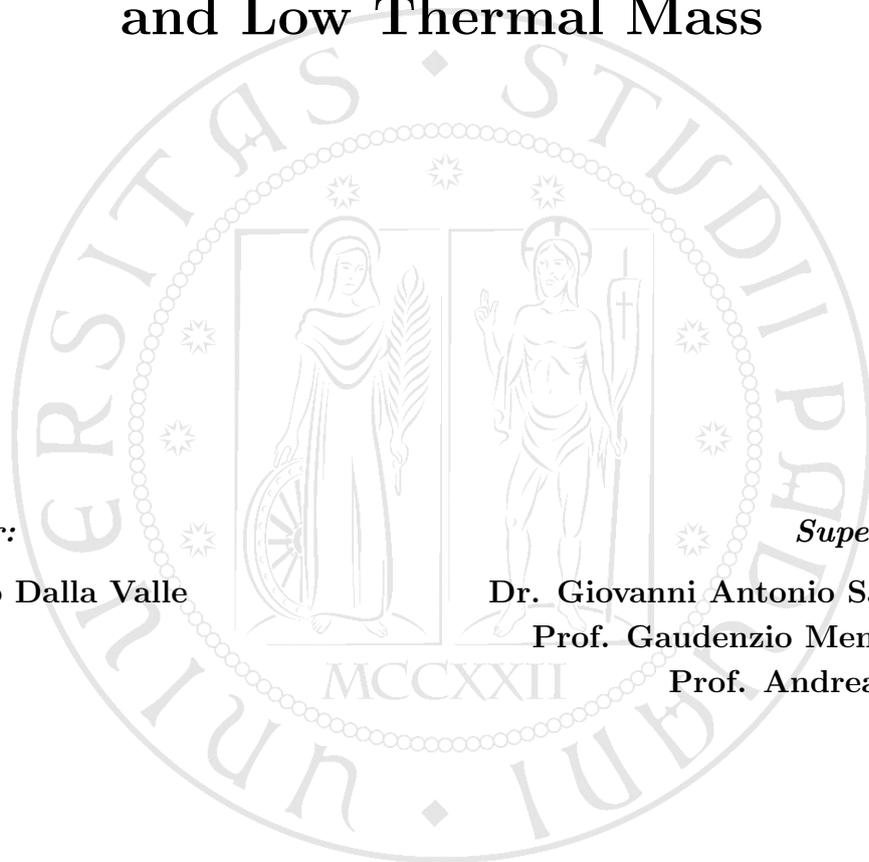
Master's Thesis

Fully Biodegradable Temperature Sensors with High Mechanical Stability and Low Thermal Mass

Author:

Filippo Dalla Valle

Superivsors:
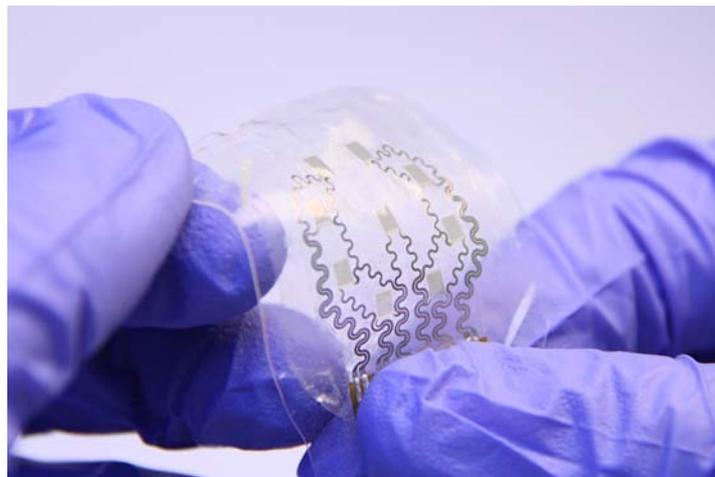
Dr. Giovanni Antonio Salvatore
Prof. Gaudenzio Meneghesso
Prof. Andrea Cester

Abstract

A general goal in the development of any electronic device is to achieve high performance operation and mechanical robustness which undergo negligible change over time. However, recent advancements in material science and thin film processing have prospected the possibility of other forms of electronics. Materials and devices are designed to provide the desired performance for a prescribed timeframe and then physically disappear via resorption by the body or the environment. In this work we have successfully designed, fabricated and extensively characterized a flexible and stretchable temperature sensor that biodegrade in the environment. The design is based on a ultrathin resistance temperature detector (RTD). The core material used is Magnesium, which is transient and biocompatible material. It has been encapsulated from both sides with a transparent and degradable elastomer produced from potato and corn starch and polylactic acid. The sensor has a variation of 70 kΩ/$^\circ$C, a resolution of 50 mK and 6 ms of response time. It shows high mechanical stability and a transient time of two months. Suddenly the device has been improved integrating 9 sensors in a single device to allow temperature mapping. A fluidic device with some channel has been fabricated to test the heat distribution during the flow of a hot fluid.

Keywords: *resistance temperature detectors (RTDs), Transient Electronics, Transfer Printing, Magnesium (Mg).*

Contents

List of Figures

List of Tables

Acknowledgements

Chapter 1

Introduction and Motivation

We live in a world where the lifetime of electronics is becoming shorter, now approaching an average of several months. Some 41.5 million tons of electronic waste was generated in 2011, and that number is expected to rise to 93.5 million by 2016, according to the research firm MarketsandMarkets. Right now, 70 to 80 percent of all that old gadgetry goes straight to landfills. This poses a growing ecological problem. Plastic consumption and waste are two of the major concerns in the modern world. Polyethylene for example is currently the leading plastic material, with a global consumption of about 83 million metric tons in 2010. Plastics normally biodegrade very slowly, with full degradation occuring after 500 or 1000 year [1]. In the race to reach the highest level of performance and realize attractive new consumer products, the issues of biodegradability and biocompatibility of the materials employed in traditional electronics are often not considered.

For this reason in the last few years the scientific community has increased the interest to move towards new frontiers in electronics, as regards materials, manufacturing techniques, leading to totally new devices with surprising features.

"Green" electronics represents not only a novel scientific term but also an emerging area of research aimed at identifying compounds of natural origin and establishing economically efficient routes for the production of synthetic materials that have applicability in environmentally safe (biodegradable) and/or biocompatible devices. The ultimate goal is to create paths for the production of human and environmentally friendly electronics in general and the integration of such electronic circuits with living tissue in particular.[2]

A novel approach to "green electronics" is the so called *Transient Electronics*: Engineering of electronics devices with the goal of achieving systems that physically disappear at prescribed times and at controlled rates. Never forgetting attention to high-performance. Applications that could exploit this transient behavior include implantable medical diagnostic and therapeutic devices that resorb in the body to avoid adverse long-term effects, fieldable environmental sensors that dissolve to eliminate the

need for their retrieval, and portable consumer devices that decompose to minimize the costs and health risks associated with recycling and the management of hazardous waste streams.

State of the art   Even if a lot of work has been done on the study of the dissolution dynamics of the materials, much less has been done on the fabrication of device and circuits. Transient electronic devices have been reported only few years ago. Thin film transistors and diodes have been fabricated with different semiconductors including organics [3], silicon [4] and oxides [5, 6]. Passive components like capacitors and inductors have been also realized but they have not been yet exploited for sensing. Important milestones in this field are: the first silicon transistors which dissolve in water demonstrated by Rogers' group in 2009[7]. Bao's group in 2010 reported an organic biodegradable transistor on a poly(L-lactide-co-glycolide), PLGA, substrate[8]. Another remarkable advancement arrived in 2012 when Rogers' group shows fully dissolvable, high performance and scalable silicon-based components which dissolve in water at 37°C [4].

1.1   Description of the work

Realization   The project lasted 6 months and was carried out in Wearable Computing Lab (ife) at the Swiss Federal Institute of Technology in Zürich (ETH) in the framework of the Swiss European Mobility Programme (SEMP). During the work I had the possibility to access to sophisticated and state-of-the-art equipment in cleanroom facilities at ETH (FIRST Lab) for the microfabrication process and to the advanced characterization tools of the Electronics Lab (IFE). Given the nature of the project a tight interaction with scientists from mechanical and biological science laboratory at ETH has been established for device specification assessment and testing.

Goal of the project   Temperature is a key parameter in living organisms which try to adapt their temperature, from vegetal to animals. Detecting the temperature with new tecnique could pave the way to new frontiers in science. The research of this project will focus on the realization of arrays of biodegradable temperature sensors for long-term and continuous monitoring in applications that require precise, fast and surface-conformal temperature mapping. Some examples include: mapping of temperature of plant leaves to studying the dynamics of plant growth combined with biochemical degradation which avoid the retrieval of the devices; thin conformal epidermal devices for noninvasive, precise, and continuous thermal characterization of human skin in critical condition (e.g. after surgery). Indeed at present, the prime methodologies for temperature rely on automated image processing of time-lapse records [9] . Such techniques require bulky and expensive tools (infrared-camera) which limit the study

to laboratory set up and to restricted area. In this project we will study materials, mechanical and electrical designs to build sensors which can be simultaneously placed on plant leaves leaves, roots or even human skin to achieve an intimate and robust contact for effective sensing and dissolve after a prescribe time. Thin magnesium layers shaped in a serpentine-like geometry will be investigated as resistive temperature sensors [10].

Idea Microfabricated resistance temperature detectors (RTD) serve as an optimal tool for measuring temperature. In fact, the extreme flexibility due to the low thickness gives them extreme flexibility and allows high compliance/conformability with the underlying substrate and adapting to every surfaces. In addition low thermal mass allows to achieve small response time.

We introduce a novel thin-film resistive temperature sensorwhich is highly deformable and fully biodegradable since it is composed by magnesium (Mg), silicon dioxide (SiO_2) and silicon nitride (Si_3N_4) and the biodegradable elastomer ecoflex (Young's modulus = 533MPa).

High spatial resolution is given by a high resistance ratio between sensing part and electrical interconnection and the low response time was ensured by extremely low thermal mass. Bendability (1.75mm bending radius) and stretchability (up to 16.9%) properties was demonstrated thanks to the devices' overall thickness of 32um and a layout of thin-film magnesium in a fractal peano-curve design.

The fabrication process was based on transfer printing in which the device is first microfabricated on a rigid substrate (e.g. glass or silicon) and then transferred on any desired substrate. Our process starts covering a silicon wafer by a stack of acetone-soluble poly(methyl methacrylate) (PMMA) and mechanically stable polyimide (PI). After subsequent pro- cessing with UV lithography tools, etching, and metal deposition PMMA was dissolved in acetone enabling the device to be easily picked up using water solvable cellulose-based tape and then transferred to the ecoflex substrate.

After the fabrication process a long period of characterization started. First a estensive study on substrate properties was carried out from electrical optical mechanical and toxicological points of wiew. After fabrication the devices were characterized in terms of electrical, mechanical and chemical performance.

An important part of the work is the study of the dissolution of the materials used to fabricate the sensors. The dissolution rate of metals (Mg, Zn), dielectric (SiO_2 and Si_3N_4) and substrates (ecoflex BASF) was studied in order to tune the transience of function of our device.

1.2 Organization of the Thesis

This thesis is divided in 7 chapters whose content is briefly reported in the following:

1. The first chapter introduces the topic of the Thesis.

2. The second chapter reports the design of the temperature sensor and describes the choice of the materials for transient electronics, with particular focus on biodegradable polymers. Furthermore it illustrates the process flow which has been implemented to fabricate the devices.

3. The third chapter explains how bendability, stretchability and resistance to hard environmental mechanical condition has been tested to benchmark the sensor from the mechanical point of view.

4. The fourth chapter reports the thermal characterization of the fabricated devices: calibration of the sensor necessary to relate electrical quantities to physical quantities (temperature), the sensitivity to temperature variations, response time and thermal stability over time.

5. The fifth chapter describes the fabrication of an array of 9 sensor and integrate it on top of a biodegradable fluidic device for flow mapping.

6. The morphological dissolution study of both stand-alone and fully encapsulate device are discussed in the sixth chapter, and a solution for biodegradable wiring is showed

7. The seventh chapter concludes the thesis by summarizing the main points of the work and giving some insights about possible future developments and applications.

Chapter 2

Materials, Design and Fabrication

In this chapter, the methodology of the present work is described. Therefore, three sections are present: the first one explains how the materials were chosen, the second one reports the design of the single sensor, while the third one shows the fabrication flow.

2.1 Materials

Transient flexible and conformable electronic needs conductors, dielectrics and substrates as conventional electronic but they all have to degrade over the time. Some material typically used in conventional electronic are still available for transient applications because they are transient. Here we shortly describe the palette of materials categorized in three classes: metals, dielectrics and polymers

Metals As shown by L. Yin et al. [11] several metals dissolve in DI water. Some examples are Magnesium (Mg), Zinc (Zn), Iron (Fe), Tungsten (W), and Molybdenum (Mo). The dissolution dynamics is typically enhanced by temperature and pH of the environment. For our application Magnesium has been chosen as conductive material. Mg is easily to etchable in HCl solution and has a dissolution rate of 0.3um h^{-1} DI in water and even higher where chloride ions are present. An other big advantages of this metal is its biocompatibility showed by D. Xue et al. [12] that is a good requisite in the framework of implant and in-body applications.

Dielectrics On the other hand some dielectrics are needed in order to prevent short circuit and leakage currents. Silicon oxides and nitrides are key materials for dielectrics and encapsulation layers in a class of silicon-based high performance electronics that has ability to completely dissolve in a controlled fashion with programmable rates,

when submerged in bio-fluids and/or relevant solutions [13]. Indeed they are essential for high performance transistors and capacitors. For that reasons they have been use in this project. In addition they have a lower dissolution rate with respect to Mg and so as to extend the lifetime of the device when used for encapsulation.

Polymers   Cellulose, gelatin, Poly(lactic acid) PLA and Ecoflex are just few of the biodegradable polymers that have been use in the past for transient electronics [14]. In Table 2.1 a brief review of their most important property is reported. For example PLA shows big advantages in terms of processability and biocompatibility. However it is bendable but not stretchable. The polymer that best fits our needs is Ecoflex, a certified compostable polymer from BASF Company. Its mechanical electrical and optical properties will be analyzed in the next sections. In addition a cytotoxicity study has been carried out.

Table 2.1: Substrate comparison

	Unit	ECOFLEX [15] 50um	NATIVIA[16] 50um PLA based	NatureFlex 42um [17] Cellulose based	PDMS [18]	Gelatin [18]
Mass density	g/cm^3	1.25 - 1.27	1.24	1.44	0.965	1.35
Melting point/heat seal	°C	110 - 120	85 - 140	not applicable	not applicable	
Transparency	%	82				∼100
Haze	%		1.8	3.0		
Gloss(45 °)	Gloss		80	100		
Tensile Strenght	N/mm^2	35/44	(MD - TD) 105 - 205	(MD - TD) 125 - 70		
Elongation at break	%	560/710	(MD - TD)[1] 185 - 85	(MD - TD) 22 - 70		
Young's Modulus	Mpa	533 (5% secant)		(1% secant) 3000 - 1500	0.36 - 0.87	0.033 (5% secant)
WVTR [2]	g/(m^2 d)	135	170		67.54 - 9.46 [3]	
OTR [4]	cm^3/(m^2 d bar)	1200	430	1 (50% umidity −>15)	37287 - 738[5]	

2.1.1   Ecoflex

Ecoflex is a stretchable, permeable, transparent and compostable polymer produced by BASF chemical company. This polymer has been choose as substrate and top encapsulation layer for the sensors.

ecofex® F Blend C1200 is a biodegradable, statistical, aliphatic-aromatic copolyester based on the monomers 1.4-butanediol, adipic acid and terephthalic acid in the polymer chain. ecofex® F Blend C1200 will biodegrade to the basic monomers 1.4-butanediol, adipic acid and terephthalic acid and eventually to carbon dioxide, water and biomass when metabolized in the soil or compost under standard conditions [15].

A big advantage of using this polymer is that ecoflex is acetone/isopropanol resistant. This offers advantages for processing with respect to cellulose or PLA foil. Furthermore ecoflex is water resistant and idrophobic, two an essentials properties that allow us to use it as encapsulation layer .

---

[1]MD: Machine Direction, TD: Trasversal Direction

[2]Water Vapor Transmission Rate

[3]depending on radical substituents (R Groups)

[4]Oxygen Transmission Rate

[5]depending on radical substituents (R Groups)

Ecoflex preparation starts from small pellets provided by the producer and dissolved in chloroform to be deposited in thin film by spin coating. Different ecoflex solution (5% 15% and 30%) have been prepared depending on the application:

5% as dielectric for thin membrane preparation [$\sim$700-800nm] (spincoating Fig. C.2)

15% mechanical substrate for sensors [$\sim$4um per layer] (spincoating)

30% bulky applications (casting)

To achieve the desidered thickness, several layers (4um each) of 15% solution have been spincoated [1500rpm/5rpm s^{-1}/60s] on glass slide. Thickness of substrates can span from 16um for ultraflexible and high-response application to 50um to obtain lower WVTR and higher shielding of the encapsulated device. Finally, to obtain freestanding membranes, the substrate were released from the slide with a little drop of water to reduce the adhesion and prevent wrinkling/curling.

2.1.1.1   Optical properties

Ecoflex optical properties have been studied by spectroscopy in the range of visible light. Since the substrate is formed by several layers of Ecoflex, two thickness of ecoflex have been tested (4um and 16um). Fig. 2.1 shows how the transparency changes increasing the thickness. Transparency has been calculated from absorbance values from the following relation:

$$T = 10^{-A} \tag{2.1}$$
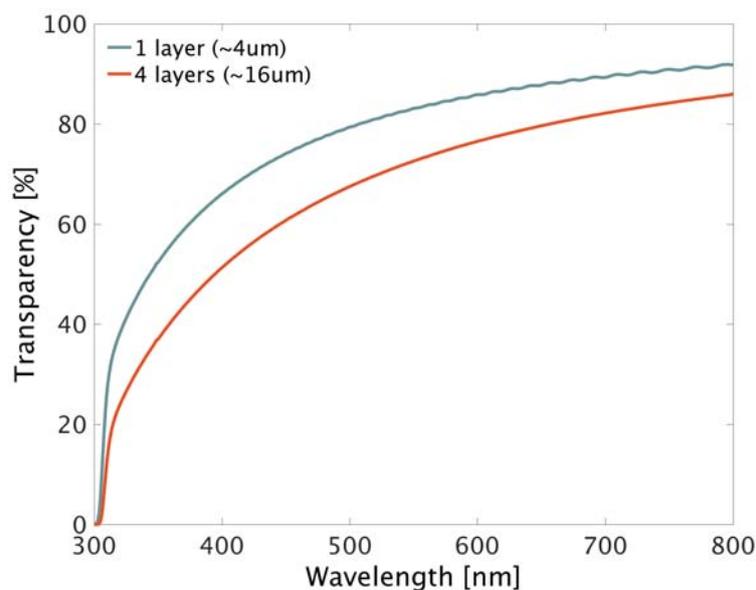
Figure 2.1: Ecoflex® transparency for two different thickness.

As shown in Fig. 2.1 Optical transparency in the visible spectre is modulated by the thickness of the material. It decreases from a mean value of 80% when ecoflex is 4um thick down to 70% when the polymer is four times thicker. It is important to note that this material shows high absorption in the UV spectrum.

2.1.1.2   Mechanical properties

The mechanical properties of a thin ecoflex membrane (thickness) have been tested upon application of longitudinal stress. The samples were prepared using spin coating to obtain thin membranes. Afterwards they were cut in to rectagular specimens with dimensions 60mm by 10mm. The thickness was measured after the experiments using a profilometer in order to compute stresses from force and deformation data. Two measurements have been defined. The first protocol looks at the viscous and plastic properties and the second one represents a quasti-static response. The material stretches are obtained using optical flow tracking of image sequences, taken during the experiment. Each material point P_k assumes the position X_k in the undeformed reference configuration. In the deformed state, the same material point is described with a position vector x_k. The experiment assumes affine deformation a-priori, which means ideally, the relationship

$$\mathbf{x}_k = \mathbf{F}\mathbf{X}_k + b \tag{2.2}$$

holds for every point P_k at every time. $\mathbf{F}$ is called *in-plane deformation gradient*. For incompressible materials, where ε_1 is the linear strain in tensile direction during uniaxial loading, from incompressibility approximation, the lateral contraction is given by constraint ($\det(F) = 1$ must hold at all times)

$$\varepsilon_{y,z} = \frac{1}{\sqrt{\varepsilon_x + 1}} - 1 \tag{2.3}$$

Figure 2.2b shows the measured lateral contraction and compares its to the incompressible response. Most rubber-like materials are assumed to be incompressible. In the case of Ecoflex however, the measurement is not expected to show accurate material strains because of a strong wrinkling effect (see Fig. 2.3a). An estimation of the Young's modulus for describing the small strain behaviour of the material, can be obtained with tangent or secant moduli. In this case a secant modulus at a strain level of 5% was used.

$$E \approx E_{0.05} = \frac{\Delta\sigma(\varepsilon = 0.05)}{0.05} \tag{2.4}$$

This allow us to conclude that Ecoflex has a Young's modulus of **533 MPa**
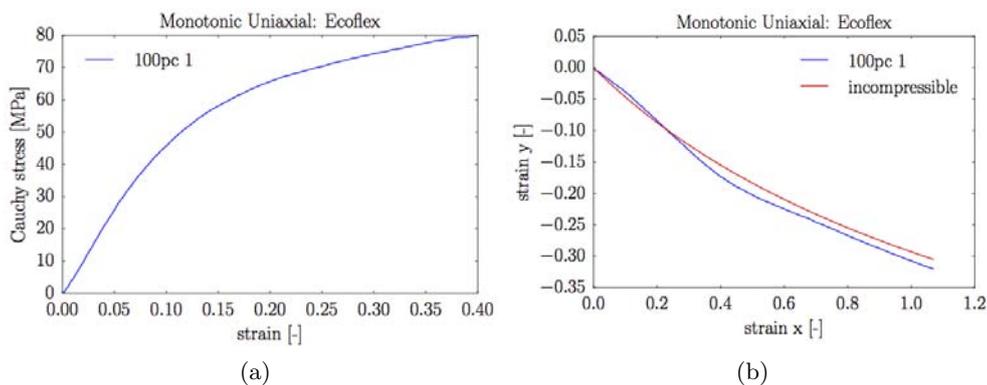
Figure 2.2: Quasi static responses. (a) Cauchy stress ("true stress") is plotted over the linear strain measure in the first principal direction. (b) Kinematic plot of quasi-static response of Ecoflex. The transverse strain is affected by errors due to the strong wrinkling effect for higher strain ranges.
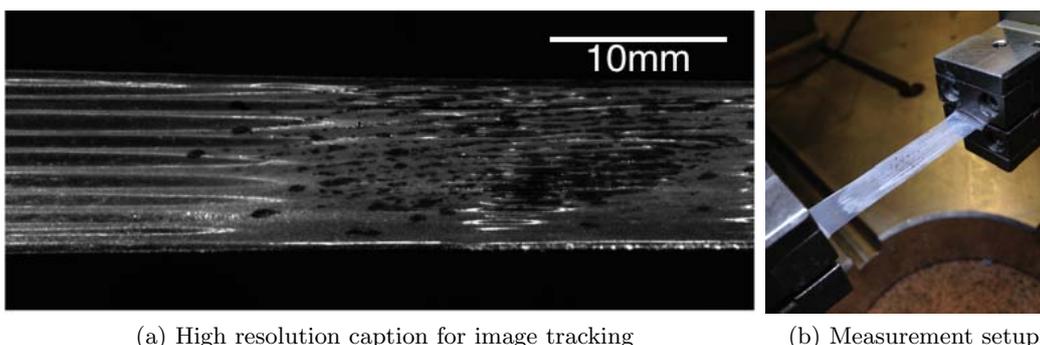
(a) High resolution caption for image tracking   (b) Measurement setup

Figure 2.3: Ecoflex® under strain during mechanical tests.

2.1.1.3 Electrical

To test the permittivity and losses of this compostable polymer an array of 6x6 capacitances have been fabricated on top of 50x75mm glass slides. Then 6 fingers 2x40mm 10nm/60nm thick Cr/Au were evaporated as bottom electrodes through electron-beam evaporation by means of shadow mask. Later a 800nm thick layer of 5% w/v Ecoflex solution in Chloroform was spincoated [6000rpm/6rpm s^{-}1/60s] as dielectric layer. Finally a second evaporation of 10nm/60nm Cr/Au as second electrode has been done using the same mask rotate of 90 degrees. Fig. 2.4 shows the fabricated devices, while in Fig. C.1 the magnified view of one capacitors is reported.
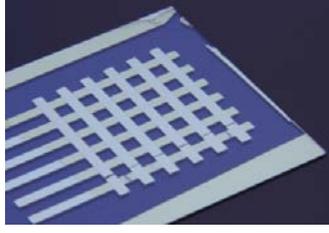
Figure 2.4: Array of capacitors fabricated on glass slide.

Using a semiconductor Device Parameter Analyzer (Keysight B1500A), both C-f and I-V measurements have been done to characterize Ecoflex properties as dielectric.
A plate capacitor filled with a homogeneous dielectric can be described by a complex permittivity

$$\underline{\varepsilon} = \mathrm{Re}(\underline{\varepsilon}) + j\,\mathrm{Im}(\underline{\varepsilon}) \tag{2.5}$$

Its real part describes the ratio of the complex amplitudes of electric flux density (displacement D) and field strength E. The imaginary part comprises all dielectric losses due to the conductivity σ of the medium. The loss factor in a dielectric can be measured by impedance spectroscopy.

$$\underline{\varepsilon} = \mathrm{Re}(\underline{\varepsilon}) + j\,\mathrm{Im}(\underline{\varepsilon}) \iff tan(\delta) = \frac{\mathrm{Im}(\underline{\varepsilon})}{\mathrm{Re}(\underline{\varepsilon})} = \frac{\mathrm{Re}(\underline{Y})}{\mathrm{Im}(\underline{Y})} \tag{2.6}$$

With permittivity $\underline{\varepsilon}$ being a complex quantity, the capacitance can be expressed in complex notation, too [19].

$$\underline{C} = \varepsilon_0 \underline{\varepsilon_r} \frac{A}{d} = C_0 \underline{\varepsilon_r} = \mathrm{Re}(\underline{C}) + j\,\mathrm{Im}(\underline{C}) \tag{2.7}$$

Assuming the admittance model for a real capacitor, which comprises a susceptance B in parallel to a conductance G, the following calculation can be done:

$$\begin{aligned}
Y &= G + jB \\
&= G + j\omega C \\
&= G + j\omega\, \frac{\varepsilon_0 A}{t} \left(\varepsilon_r^{'} - j\varepsilon_r^{''} \right) \\
&= \omega \frac{\varepsilon_0 A}{t} \left(\varepsilon_r^{''} \right) + j\omega \frac{\varepsilon_0 A}{t} \left(\varepsilon_r^{'} \right)
\end{aligned} \tag{2.8}$$

$$\implies \varepsilon_r^{'} = \frac{t}{\varepsilon_0 A}\, \frac{\delta B}{\delta \omega} \tag{2.9}$$

From the measurement recorded with the parameter analyzer both tangent loss and $Re(\underline{\varepsilon_r})$ have been extracted (Fig. 2.5) in the range 1kHz - 5MHz. Ecoflex shows a permittivity at low frequency around 4 and the tangent loss are always below 0.07 in the range 1kHz-5MHz. Regarding the I-V measurement it was performed to test the breakdown field. No breakdown has been reported below 42V which means a field of 0.5 MV/cm since the dielectric thickness was 800nm, while some hystherisis has been observe (see Fig. 2.5b).

(a) Permittivity and losses.   (b) I-E hystheresis.
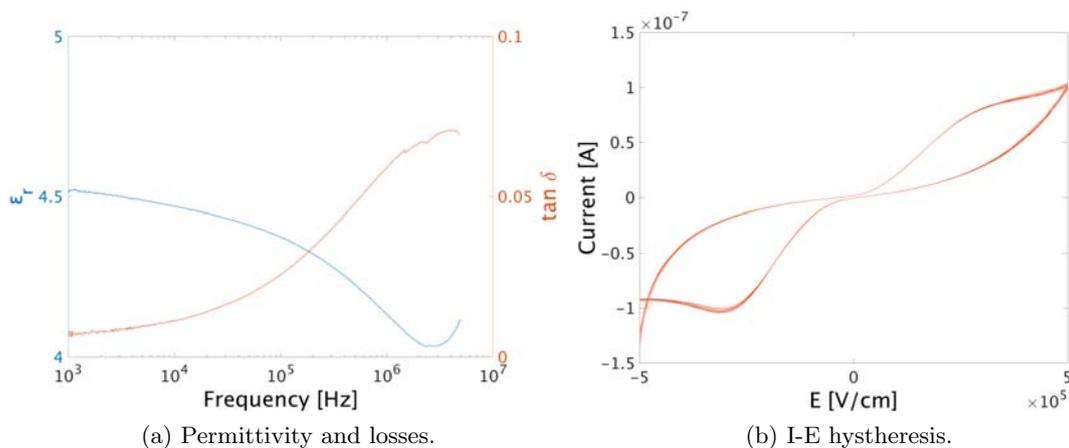
Figure 2.5: Ecoflex® electrical properties.

Fig. 2.5b shows the current in the device over the applied field. No breakdown effect has been reported below 0.5 MV/cm while there is some hystheresis over 0.1 MV/cm.

Cytotoxicity

Cytotoxicity and toxicity in general are important for environment and biodegradable application where the devices are intended to be abandoned and becomes a key point if implantable applications are considered. Biocompatibility of Magnesium, Silicon Oxide and Silicon Nitride have been already shown [13]. On the contrary although ecoflex is a certified compostable material (US standard ASTM D 6400) [15], no toxicity studies have been done in the past for it.

For this reason the cytotoxicity of ecoflex has been studied for the first time through colony-forming assay ISO 10993-5.

Cytotoxicity testing is a rapid, standardized, sensitive, and inexpensive means to determine whether a material contains significant quantities of biologically harmful extractables [20] .

In standard cytotoxicity test methods, cell monolayers are grown both on top of commercial tissue culture plastic containers (control) and the substrate under test. The difference between the two substrates shows the grade of cytotoxicity. In spite of others toxicity death/alive tests in which the grade of toxicity is determine by the percentage

of cells that survive after a fix time, in ISO 10993-5 the toxicity is related to the growth stage of the neuronal cell. In particular to the axons length. This method is more accurate and allows to deeply characterize the material's toxicity since neuronal cells are very sensitive to harmful substances.
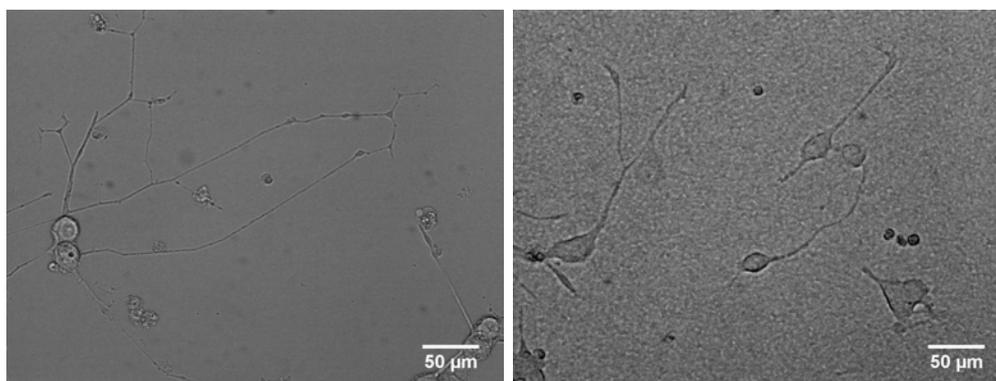
(a) neurons on control substrate   (b) neurons on Ecoflex
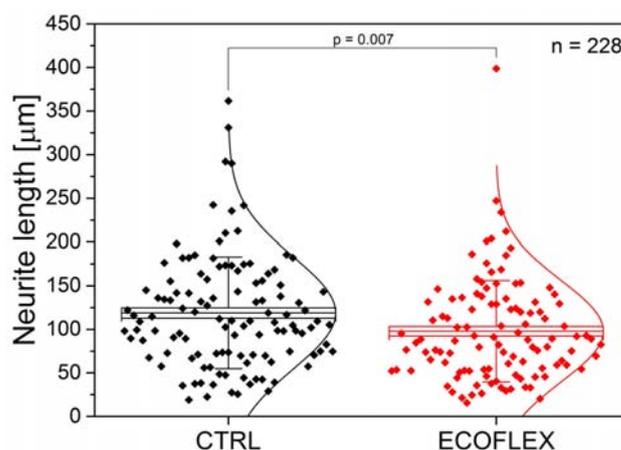
(c) Comparison between ecoflex and control substrate.

Figure 2.6: Cytotoxicity study. Ecoflex's roughness (b) is higher than control substrate (a). This is due to plasma treatment to enhance its hydrophilicity. (c) Populations comparison: the boxplot indicate the mean value and the error bars represent the standard error of the mean. Total number of measured neurite is shown at the figure legend. "p" is the estimated probability density

Protocol: 3mm diameter round glass slide cover slips have been coated with a solution of 5% v/w Ecoflex® in Chloroform, after the evaporation of the solvent (120 sec at 60C), the surface has been treated with O_2 plasma to enhance hydrophilicity and coated with a solution with neuronal cells in a early stage of growth. After one week the numbers of neuronal cells alive on Ecoflex have been counted and them neurite length has been measured and compared with the control substrate. Fig 2.6 shows neuronal cells on both substrate and a plot with the difference between the populations [21].

Results: after 1 week almost all the neuronal cells were still alive and the neurites grew properly. For our envinromental application we can state that is definitely a good result and Ecoflex can be used as substrate or dielectric in biodegradable application without relavent environmental problems. This study paves new opportunities in the use of this polymer. An example could be implantable devices. However, in this case, it is necessary to study in deep the toxicity with in-vivo implant followed by histological analysis on cells.

2.2 Design

Our device is based on Resistance Temperature Detectors **RTDs**. Many RTD elements consist of a length of fine wire wrapped around a ceramic or glass core but other constructions are also used. The RTD wire is a pure material, typically platinum, nickel, or copper. The material has an accurate resistance/temperature relationship which is used to provide an indication of temperature [22].

For continuos and fast temperature tracking a extremely low thermal mass is needed, furthermore to archive high flexibility and stretchability a planar design is necessary. The active layer of our device is a 250nm thick (t) layer of Magnesium. The temperature-sensible region (Fig. 2.10b) consists in a stripe of Mg folded 100 times in a serpentine-like shape and arranged in a rectangular 2x2.5mm. It is 10um wide (W) with an overall length (l) of 25cm long. It acts as RTD. The theoretical values can be calculated from:

$$R = \rho \frac{l}{t \cdot W} \tag{2.10}$$

Interconnection adopt a fractal design to achieve high stretchability. A peano-based design has been choose for that purpose. Peano-based layouts show to be highly resistant to external strain. Half-and-Half peano-curves provide a stretchability of 16% in x-axis and of 13% in y-axis [23].

An other key point for precise spatial sensing is the resistance ratio between the core of the device and the interconnections. For that purpose the interconnections has been designed to have negligible resistance with respect to the serpentine trace. The interconnections are about 5.5cm long and 300um width (average values). This give a $\frac{R_{sense}}{R_{connect}}$ ratio above 130. This allow us to conclude that the temperature is sensed only in the serpentine spot without influence of the contact and interconnection resistance. Since the device will be fabricated on silicon substrate a transfer onto the final substrate will be needed. Transferring such a very small traces 10um wide is critical. For that reason two layers of insulator SiO_2 and Si_3N_4 respectively have been designed all over the sensor to improve mechanical stability.

(a)   (b) zoom on traces
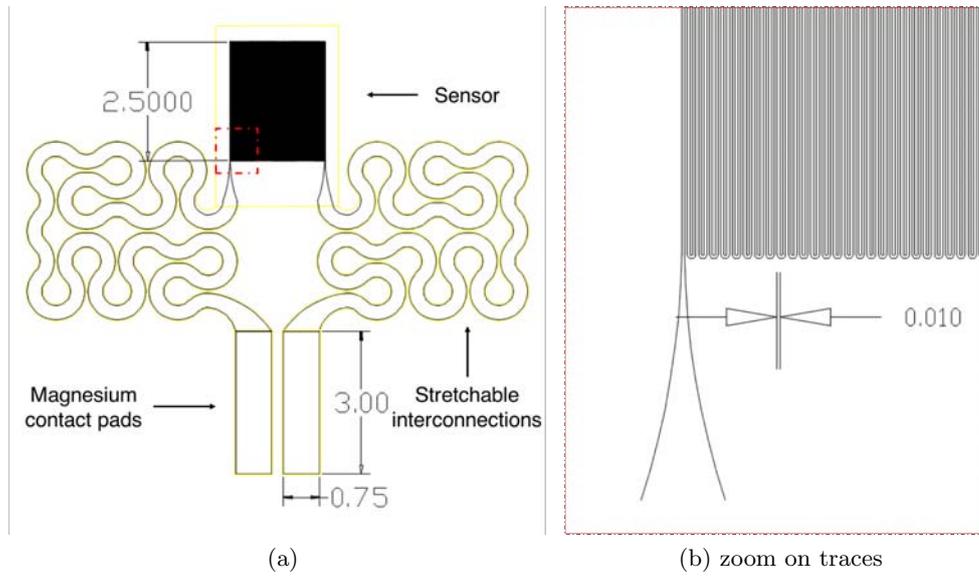
Figure 2.7: Design of the sensor. Dimensions in mm.
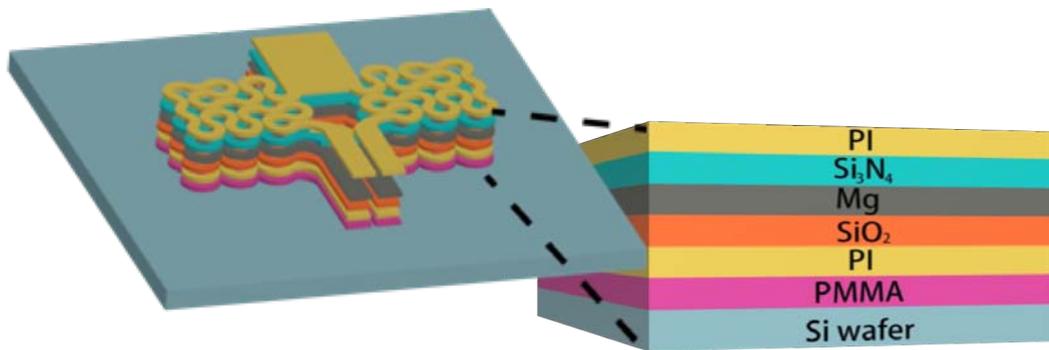
Figure 2.8: Stack of all layers of before transfering. Silicon nitride layer won't deposited on pads so that after PI top etching will be possible to get electrical contact.

2.3   Fabrication

In this section the most relevant steps of the fabrication flow be shown. A list with all fabrication steps in detail is present in appendice A, Tab A.1 Microfabrication of devices directly on thin soft and flexible substrate (e.g. Cellulose PLA Ecoflex ecc.) which are the typical requirements for wearable application is quite critical. This is due to principal two reasons. First is their low melting point (around $100°C$) and second is that they are typically not resistat to water and solvents. In fact a lot of fabrication steps developed for conventional fabrication processes (such sa lithography, electron beam evaporation, lift-off, chemical vapor deposition etc.) require both thermal and mechanical stable substrate and resistance to solvents. Transfer printing has been used to overcome these problems. Transfer printing [24] is a process in microfabrication that

(a) Fabrication on sacrificial layer

(b) Dissolution sacrificial layer

(c) Pick-up with dissolvable tape

(d) Etching of mechanical stable substrate

(e) Transfer on final substrate
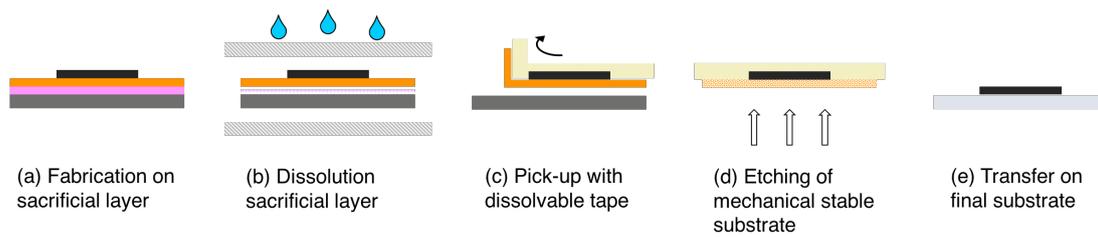
Figure 2.9: Transfer printing tecnique (with etching step in between)

allows existing devices to be transferred from a Si wafer to a receiving PDMS or tape substrate by a single peel-off step [25] and then onto the final substrate. Some key point of the transfer printing tecnique are illustrated in Fig. 2.9. The fabrication starts from silicon wafer where a sacrificial layer (SL) and a mechanical stable layer (polyimide) are deposited by spincoating respectively. On top of mechanical layer that serves as a foundation for further steps some conventional process has been done. Starting from deposition of 100nm Silicon Oxide (SiO_2) by PECVD (plasma enhanced chemical vapor deposition) and then 250nm sputtered Magnesium (Mg). After the patterning of the resist by lithografic process, Mg layer has been etched (Fig. 2.10) by wet etching with 10mMol HCl solution. Then a second encapsulation layer 100nm thick of Silicon Nitride has been deposited on top of the structure by PECVD masking the contact pads (see. A.1), plus an other layer of polyimide to avoid stress and cracks during the transfer process was deposited. Finally, after patterning, all the stack was etched by dry etching (Reactive Ion Etching). This conclude the fabrication on Si substrate.
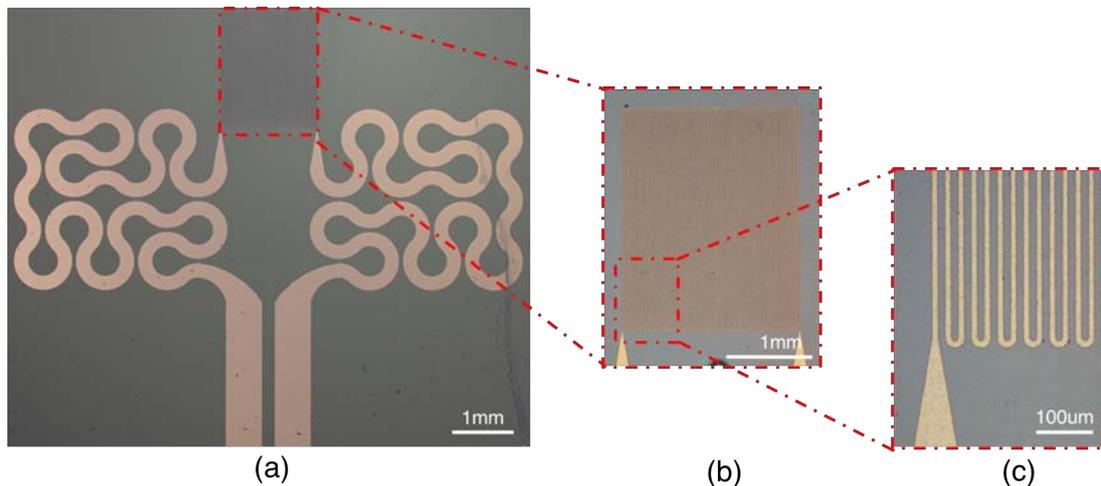
Figure 2.10: (a) Device on Silicon substrate after Magnesium etching. (b) Zoom on sensing part. (c) Particular on sensor traces (10um wide).

The fabrication flow (Fig. 2.13) continues with the dissolution of the sacrificial layer. The device was clamped between two glass slide wrapped with wipes and put in acetone overnight. After dissolution of SL the structure that was laying on top of Si wafer with

poor adhesion was picked up with dissolvable cellulose tape. Before transfer on final substrate RIE etching of polyimide was needed to remove the mechanichal-support layer. Later, after transfer of the sensor on ecoflex substrate, the last RIE etching process was needed to remove the top PI layer as well and expose Mg over pads to allow electrical contact for testing. The fabrication ends by wiring the sensor and a top layer of ecoflex to encapsulate the device.

(a) Device on   (b) Lamination of   (c) Heat sealing
final substrate   top ecoflex layer   on hotplate
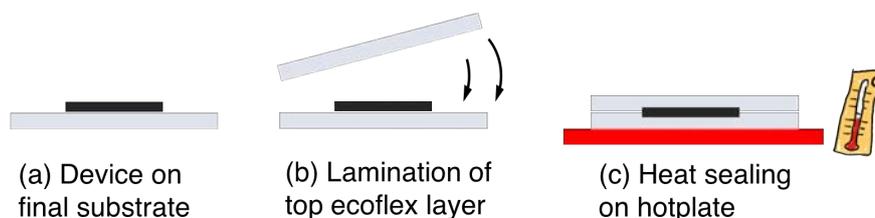
Figure 2.11: Encapsulation tecnique to enlarge lifetime.

There are at least three good reasons that suggest the need of pack the devices among layers of the same thickness (encapsulation). The first is slow down the transient time of the device and enlarge its operation lifetime. The second is that those layers (tipically polymers) act as a shield from environmental. Moreover, as the encapsulation layer has the same thickness as the substrate, the sensor will be located in the neutral strain position (where bending-induced compressive and tensile strain cancel each other) [26] which means they are not subjected to strain and thus are highly stable during sharp bending. For this purpose Ecoflex has been use. It is not only the substrate of our devices but act also as barrier to water and vapor. In addition it is transparent, a properties which is often necessary or at least a plus. Fig. 2.11 shows the main step about the deposition method of the top encapsulating layer. (i) lamination of a freestanding film previously prepared by spincoating. (ii) heat sealing of the two membranes on hotplate at 135°C. Fig. 2.12 shows the 3D model of the final device.
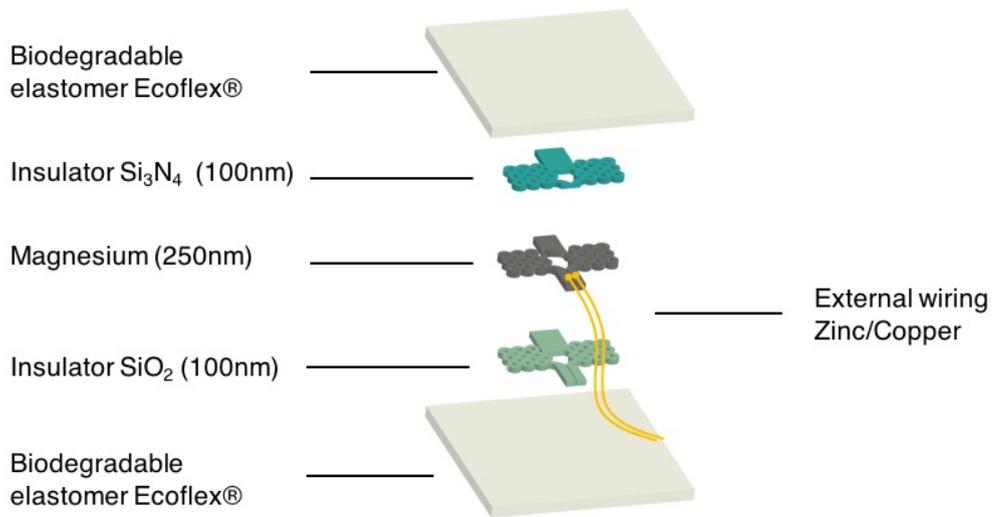
Figure 2.12: 3D Model of final device. The active layer (Mg) is first surrounded by SiO_2 and Si_3N_4 [note the difference between the upper and lower layer to allow wiring]. Then these three layers are encapsulated in two polymer films (Ecoflex).
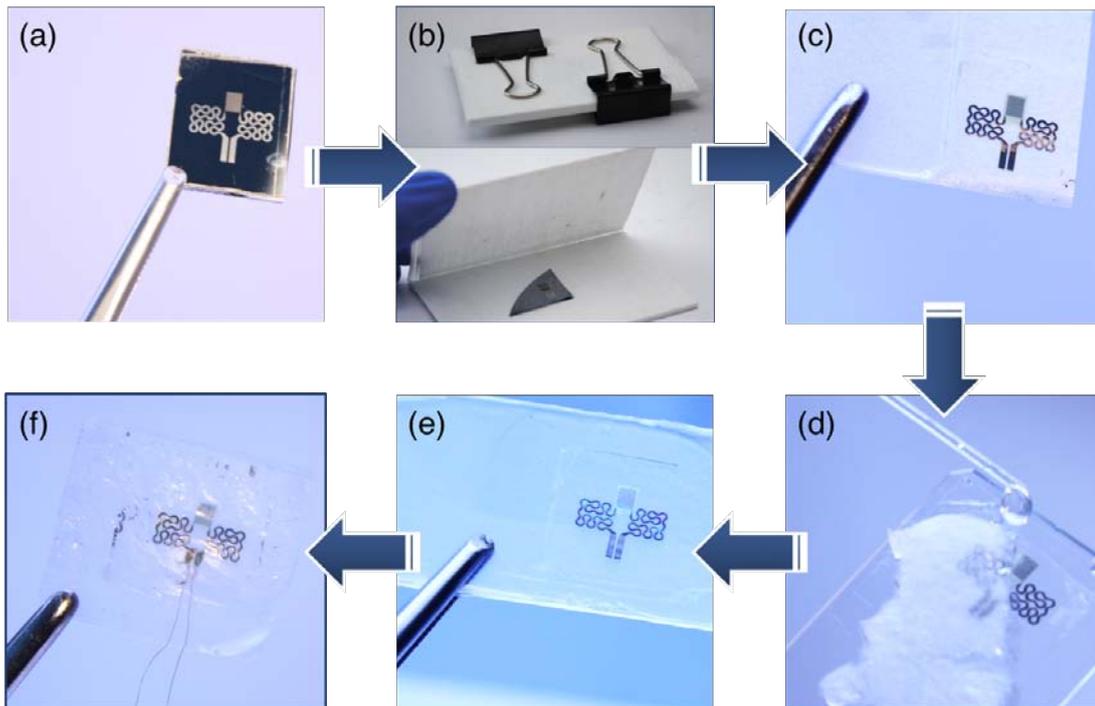
Figure 2.13: Fabrication flow. From silicon substrate to final device. (a) Device on fabricated on silicon and ready to be transfered. (b) Sensor clamped between glass slide wrapped with wipes to dissolve sacrificial layer (PMMA). (c) Device picked-up with cellulose tape after PI etchig [top layer]. (d) Transfering on ecoflex and dissolution of cellulose tape with DI water. (e) Sensor on ecoflex after PI etching [top layer]. (f) Device wired and encapsulated with ecoflex top layer.

Chapter 3

Mechanical Characterization of the Device

This chapter reports the results of the mechanical characterization of the device. First some hard mechanical stress have been carried out to test the limit of the device. Then the following section shows the bendability properties of the sensor wrap around rods from 6mm down to 1.75mm radius. The last part shows the stretching properties in both X and Y directions up to 10% strain.

3.1 Hard mechanical stress

As shown in Fig. 3.1 the sensor was either completely folded between two finger several time and crumpled in the hand. After tens of time the device was still working properly with 0.6% changing in resistance and no failure have been reported.

However, due to the nature of the tests wiring can't be done so these measurements were carried out by means of probe station. For that reason this kind of tests are intended to show only the high strength of the sensor before failure and not to characterize rigorously the sensor.

(b) Sensor folded   (c) Sensor crumpled

Figure 3.1: Mechanical hard stress.

3.2   Bending

To test how the mechanical stress due to bending affects the sensors, it was wrapped around on some metal rods from 6mm down to 1.75mm radii and the variation in resistance was tracked with a precision measure unit (Keysight B2902A) which has a resolution of 1 pA and 1 uV respectively. To avoid self heating the sensor was measured by pulsed waveform and sampled at f = 100Hz. A total of 500 points have been registered for each rods size (details in Appendix B). Obviously the rods and the clamping system temperature influence the temperature measured by the sensor. For that reason all the equipments used during the tests were put in the same place overnight to reach thermal equilibrium. Nevertheless all the manipulations of rods have been made by pincers to avoid heating. Since the variation in resistance due to bending were very low, to exclude that temperature drift in the room influences the value of the resistance, the measurements haven't been carried out from the biggest radius down to the smallest but alternating "big" and "small" radii.
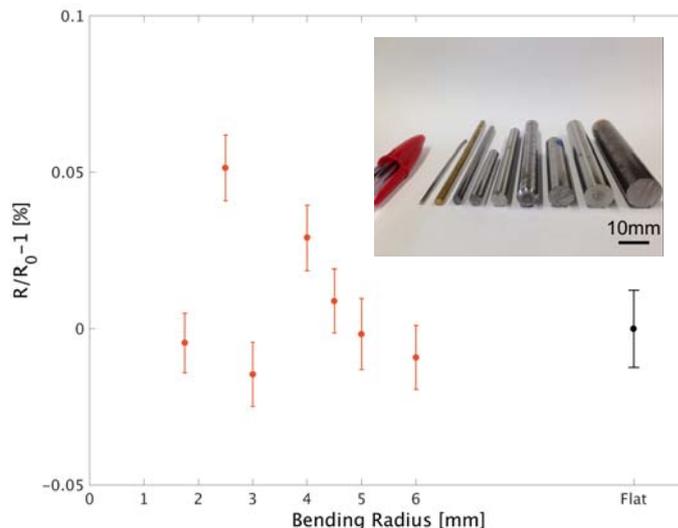
Figure 3.2: Resistance variation versus bending radius. Inset: example of some rods used

In conclusion, the maximum variation in percentage reported is 0.05% or else $\sim 15\Omega$ and this implies $0.2°C$. This variation can be imputed either to a variation due to mechanical stress or most probably to a measurement error due to temperature variation (see section 4.4 Fig. 4.3b). This, in in addition with hard mechanical tests showed before, allow us to conclude that the sensor is able to acquire correctly the temperature down to extremely low bending radii with an accuracy of $0.2°C$

3.3   Stretching

Stretchability is an other important features that all the conformale electronics should have in order to conform on soft surfaces. In our case the goal is achieved by using a thin foil of ecoflex combined with a fractal design for the interconnections.
After wiring the sensor has been mounted on a custom stretching setup (Fig. D.1) and clamped in freestanding position with no stress applied. Then with a caliber the initial position l_0 was set. Then with the stretching setup thimble the sensor was strained to the next position.

$$Strain_\% = \frac{l - l_0}{l_o} \cdot 100 \tag{3.1}$$

Regarding the acquisition protocol (voltage, frequency, Duty Cycle etc.), the measurements has been done as well as the previous case (bending).
The result are shown in Fig. 3.3 and 3.4. It's important to point out that the sensor behaves alike in both directions and survives up to 10% elongation in both directions.

In this case a trend in resistance over strain is visible and it's around 0.2% which reported in temperature is ~1°C.

(a) Resistance variation versus strain.   (b) Sensor stretched
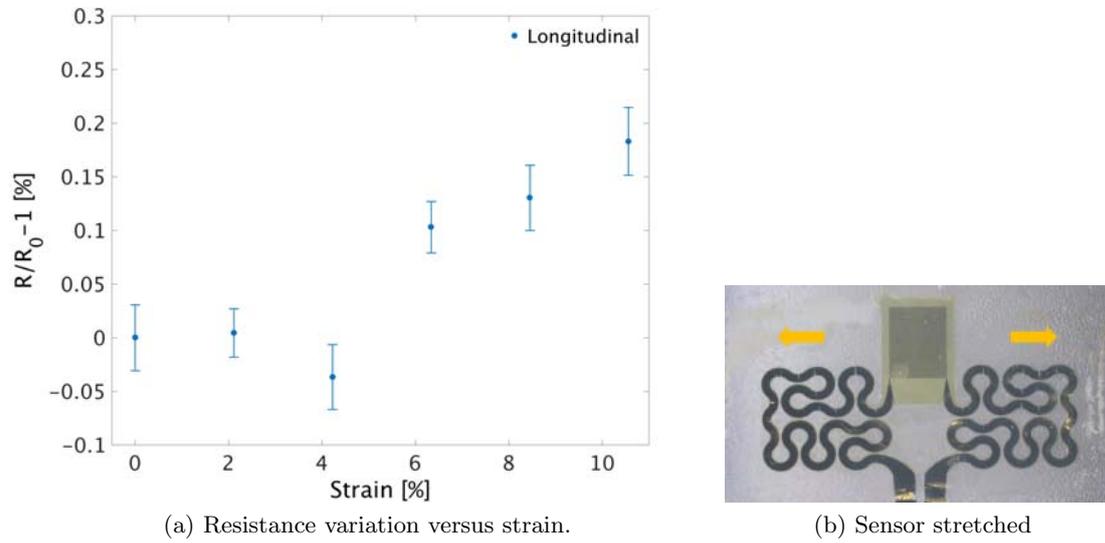
Figure 3.3: Device under longitudinal strain.

(a) Resistance variation versus strain.   (b) Sensor stretched
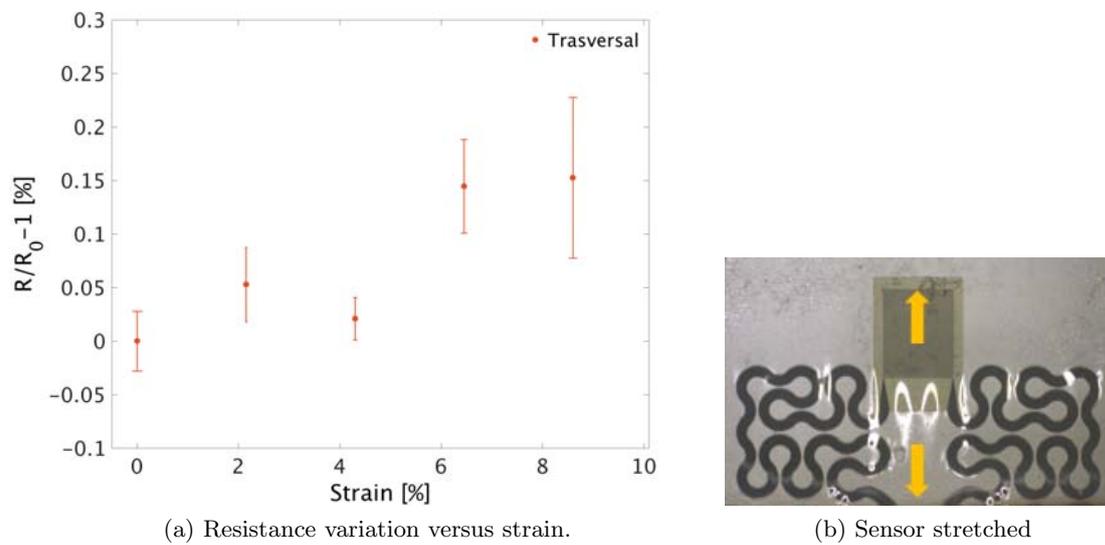
Figure 3.4: Device under trasversal strain.

Chapter 4

Thermal Characterization of the Device

This chapter reports the thermal characterization of the device. First the thermal stability of the sensor is studied with an accurate description of the calibration set-up, then an explanation of how the calibration was carried out. In addition the response time of the sensor was measured spilling a droplet of hot liquid on top. Finally some application about contactless sensing and temperature mapping are shown.

4.1   Calibration

The calibration process for a high-sensitive temperature sensor is not trivial because of may affect the actual temperature and could corrupt the calibration process (e.g. air flow, thermal equilibrium not reached). To calibrate the sensor we need to know the exact temperature of the sensor during all the process. In order to do that first of all a high-precision hotplate is needed, usually "good" hotplates stabilize temperature in a range of 1K that is definitely not enough. For that purpose a hotplate with a resolution of 0.1K calibrated with liquid crystals was used. It was able to sabilize temperature over 0.2K that allow us to calibrate properly the sensors.

During this calibration we assume that, after a transient, hotplate and sensor are at the same temperature. For that purpose perfect contact between surfaces (no air gap) and low thermal resistance are needed. The calibration has been done after encapsulation process before release the sensor from the glass slide. In order to lower as much as possible the thermal resistance between sensor and hotplate, some thermal paste has been use between plate and glass slide (see Fig. 4.1a) Then, the sensor was covered with a plastic, transparent lid to avoid temperature fluctuations due to air flows in the room To prove that the sensor has no thermal hysteresis a double sweep measurement has been carried out. First the active heating up sweep by mean of the hotplate and the calibration was performed with 1K step, then the temperature was tracked during

the cooling down of the system with the same temperature step but with 0.5K shift. Finally we got a calibration over 30K span every 0.5K and we show the absence of hysteresis and the linearity from 20 to 50°C.

The variation in resistance is due to physical property of the material (in our case Magnesium) and it can be expressed as

$$R = \rho \frac{L}{S} \tag{4.1}$$

where ρ is the resistivity of the material and it changes with temperature by the law

$$\rho = \rho_0(1 + \alpha(T - T_0)) \tag{4.2}$$

where the temperature coefficient of resistance (α) is a property of the material. After some algebric steps we obtain

$$\begin{aligned} R &= \frac{L}{S} \cdot \rho_0(1 + \alpha(T - T_0)) \\ &= R_0 + k(T - T_0) \end{aligned} \tag{4.3}$$

The value of α was extracted by means of numerical software, and amounts at 2.45 $\cdot 10^{-3} K^{-1}$, which is lower than the value of 3.26 $\cdot 10^{-3} K^{-1}$ reported in literature [27]. For typical values of our sensor $\sim$30kΩ this implies a k values of

$$\sim 70\Omega/°C$$

which means a variation of 0.2 %/°C, this value is several times lower for our sensor than the commercial RTDs which have 3-4%/°C variation and this is due to material properties. In fact the commercials ones are made with other core materials like Platinum, Nickel or Copper.

Once the sensor is calibrated, the temperature can be extracted with the following relation

$$T = T_0 + (\frac{R}{R_0} - 1)/\alpha; \tag{4.4}$$

(a) sensor on high-precision hotplate   (b) Resistance variation versus temperature
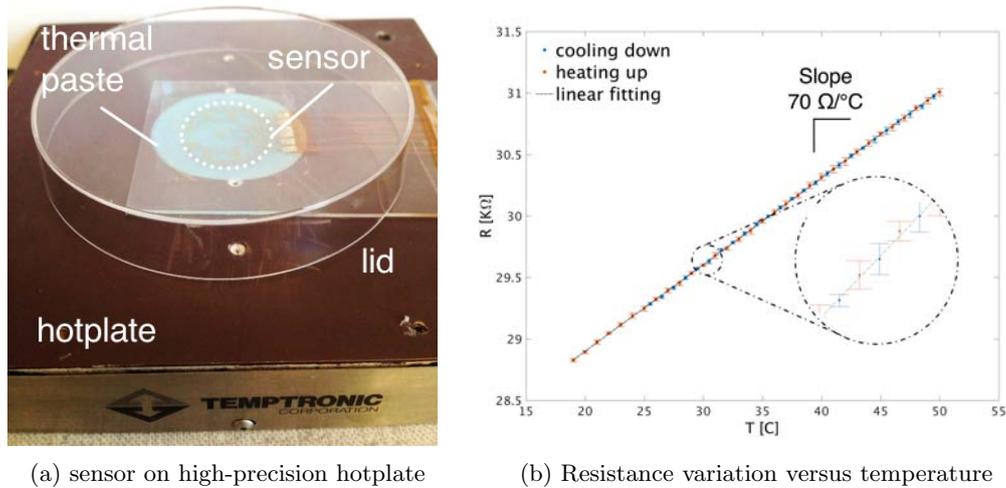
Figure 4.1: Calibration of the device. The measurement protocol consisted to set the desidered temperature, let the transient ends (180s waiting) perform the measurement over 500points with a sampling rate of 100Hz by applying a pulsed square wave of 5V with 0.4% Duty Cycle, setting the new temperature value and so on.

4.2   Sensitivity

Considering the single measurement an average to estimate the sensitivity can be done. When data is averaged, the standard deviations readings over the 5s periods is 2.855Ω for the sensor laying on a metal plate, this implies a temperature deviation of 41 mK considering a resistance variation of $70\Omega/^{\circ}C$. It was observed that the absolute accuracy of the sensors would sometimes vary between experiments while maintaining the same temperature sensitivity, which would manifest itself in a constant offset in temperature reading. This is attributed to small variations in the contact resistance between the sensor contact pads and wiring cable used to connect to the data acquisition system. Because the sensors rely on a measurement of voltage drop through the circuit, a change in the contact resistance of the wire leads should manifest as a constant offset in temperature reading.

4.3   Response Time

The response time of a measuring instrument is often ignored because it is generally much less than that of the system under investigation. In some situations, however, this is not necessarily a good assumption. It is defined as the time it takes to read 63.2% of a step change in temperature. Typically this measurement is made by plunging a sensor at room temperature into a bath and noting the time required to reach 63.2% of that step change. Generally speaking, it takes approximately five time constants before 100% of the step change is realized. For ultrathin lightweight temperature sensor response time

Material	Thickness [nm]	Density [$g \cdot cm^{-3}$]	Specific heat capacity [$J \cdot g^{-1} \cdot K^{-1}$]	Thermal mass [$uJ \cdot cm^{-2} \cdot K^{-1}$]
Mg	250	1.74 [29]	1.023 [29]	44.5
SiO$_2$	100	2.3 [30]	1 [30]	23
Si$_3$N$_4$	100	2.5 [31]	0.17 [31]	4.25
PLA	40000	1.24 [32]	1.8 [32]	9000
ecoflex	18000	1.25-1.27 [15]	~ 1.88 [1] [33]	4300

Table 4.1: Calculation of thermal masses of Mg, SiO$_2$, Si$_3$N$_4$, PLA, ecoflex.

is a key point. Many applications require a low response time to track rapid changes in temperature. For example R.C. Webb et al. in 2015 showed that a ultrathin, soft, skin-conforming sensor can be use for blood flow mapping [28]. In that case the device consists of a single thermal actuator surrounded by two rings of temperature sensors. The central thermal actuator provides a constant source of thermal power to create a mild, well-controlled increase in temperature at the surface of the skin in the vicinity of a targeted vessel. Then the rapid variation in temperature was tracked by the thermal sensors. A small response time in this application is extremely important.

To guarantee small response time, extremely low thermal masses are necessary. Therefore, the thermal mass (T) of a single sensor was calculated from the thickness (t) of each layer, its density (d) and the specific heat capacity (C) as $T = t \cdot d \cdot C$. Single masses of layers are listed in Table 4.1

It results in a total thermal mass of $\sim$**72** $\mu J \cdot cm^{-2} K^{-1}$ for the standing-alone sensor and approximately **4.4** $mJ \cdot cm^{-2} K^{-1}$ for a device fully encapsulated. Due to its very low thermal mass, the sensor has expected a small response time.

To test this property, the sensor was released from the glass slide and clamped on a custom stretching setup (see Fig. D.1). A drop of warm liquid has been put on top of the sensor by means of a pipet see Fig. 4.2b. Water can't be used for this purpose because the sensor would dissolve. Since Isopropanol was used for many fabrication processes and doesn't damage the sensor, it was used to test respose time. In addition, due to its high volatility it evaporate very fast and allows us to perform multiple response time tests. The sampling frequency has been set to 1 kHz. Higher sampling rates wouldn't help because the multimeter has a minimum pulse width of 400us. Increasing the frequency would implied a higher Duty Cycle with an increasing of the power dissipated and consequently self heating problems.

The measured response for our sensor is **5.9 ms** (see Fig. 4.2a). If we consider the time it takes to reach 90% (defined as the rise time) this value increase to 9.1 ms. This is a extremely small response time if we compare this value with commercial RTDs. Usually they have a response time of 1-2 sec. This means that our sensor is two orders

---

[1]Exact values not provided by producer. Copolyester value was used.

of magnitude faster than commercial ones.

(a) Single rise time. (b) Device under test
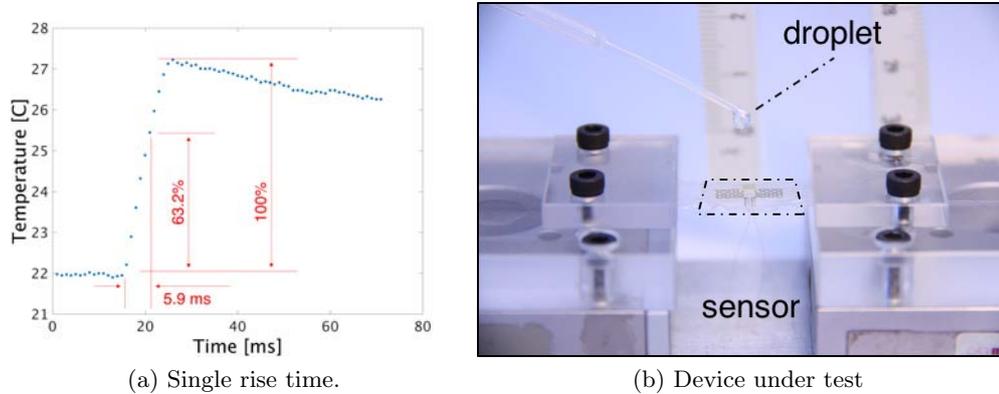
Figure 4.2: Temperature variation induced by droplet of Isopropanol warmed up to 30°C.

4.4 Thermal Stability

Thermal stability is extremely important for long term and continuous tracking of the temperature. So that two kinds of measurements has been done.

First the sensor was put on top of a high-precision hotplate (the same used for calibration process) set at constant temperature. It was covered with a lid to keep the temperature as constant as possible and ensure the minimum variation in temperature from the environment. The test has been repeated for three temperatures: 26, 25.5 and 26 to highlights eventual drifts. No temperature drift have been sensed from the sensor. Fig. 4.3a shows temperature fluctuation due to the hotplate to keep the temperature constant. In fact they are in the 0.2°C range.

Second the temperature registered from the sensor laying on top of the desk in a "standard room" was tracked over the same time span.

The difference between the two graphs 4.3 shows how much the room temperature can change temporary and instantaneously due to passage of a people or a air flow.
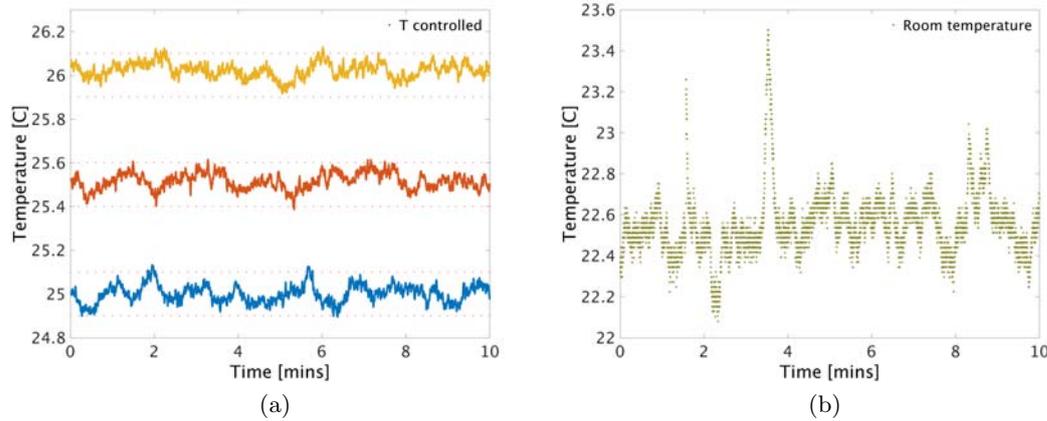
Figure 4.3: Long measurement (10 minutes) to test thermal stability of the sensor. (a) The variation in temperature measured by the sensor stays in the hotplate stability range (0.2°C). No self heating have been reported. (b) Variations in temperature registered in the room.

4.5   Applications

High sensititive, lightweight and compliant temperature sensors find a lot of applications in science and in industry to test other physical quantities instead of pure temperature. Two examples have been reported in this work in the following sections. First temperature sensor use as proximity sensor will show

4.5.1   Contactless sensing

Due to its extremely low thermal mass those sensors are able to sense the temperature variation imposed without contact.

Fig. 4.4 shows how the resistance variation can be related to the presence of a human finger. This variation can be related to temperature variation. In case of a finger the increase in temperature sensed by the sensor is in the range of 1-1.5 °C when it was 1 cm away from the sensor. The test has been repeated several times over 3 mins and Fig. 4.4 shows the high degree of repeatability and the absence of temperature shift due to heating of the entire system. Another experiment has been carried out to further analyze contactless effect. A standard desk lamp (power 60 W) was used for this experiment. It was placed at different heights and turned on and off. The graph shows the temperature variation. For example these data can be used to detect the lamp status (ON/OFF). With this setup the maximum distance in which the sensor is able to detect the lamp status is 40 cm. In addition the sensor can be used as proximity sensor since a relation between temperature and distance can be extracted.
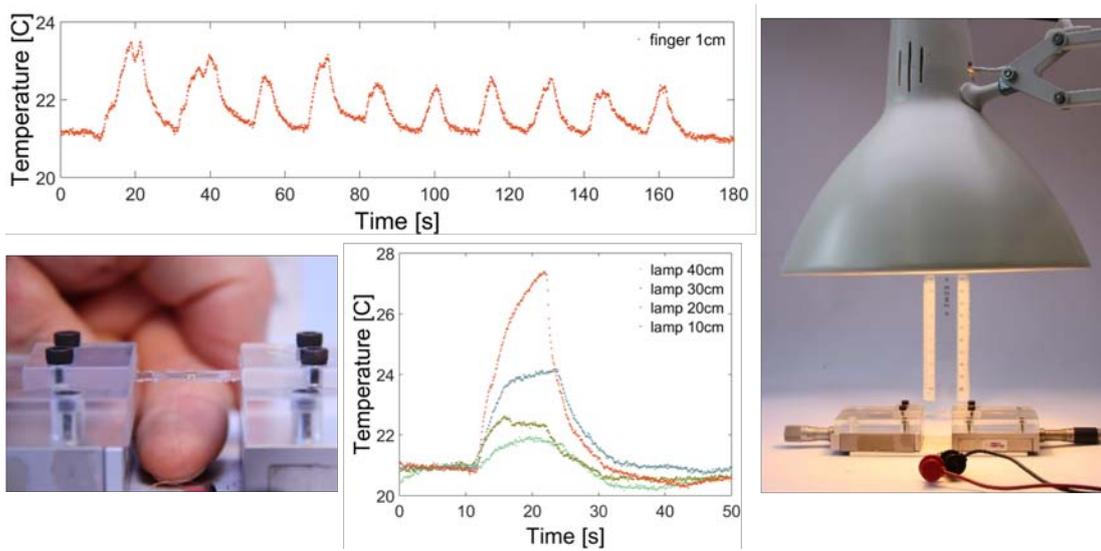
Figure 4.4: Sensing with contactless technique.

Chapter 5

Array and Microfluidic

In this chapter an evolution of the single sensor design will be shown. With this new design we aim to cover a wider range of applications instead of simple spot measurements. The design combine 9 sensors, 8 arranged in a octagonal shape plus one in the middle. Finally some hints about the tremendous potentially of this devices will be given. A bendable and fully biodegradable flow detector will be presented.

5.1   Design

The design consists in a array of 9 sensors. Each sensing part is designed exactly the same as the single sensor while an evolution in the interconnection has been developed in order to arrange them in a octagonal shape. The ninth sensor has been placed in the middle of the polygon (see Fig. 5.1). The overall dimensions are 20x30 mm.
From the electrical point of view the sensors are grouped into 3 isolated different circuits: left, center and right. In fact to save complexity and space four sensors share one end in a common pad. The central sensor is designed with dedicated connection to allow its use independently. This implies that 12 contact pads are present: 9 for signals and 3 common that typically will be connect to ground. The sketch in Fig. 5.2 represents the sensors' numbering and its correspondence with the contact pads.
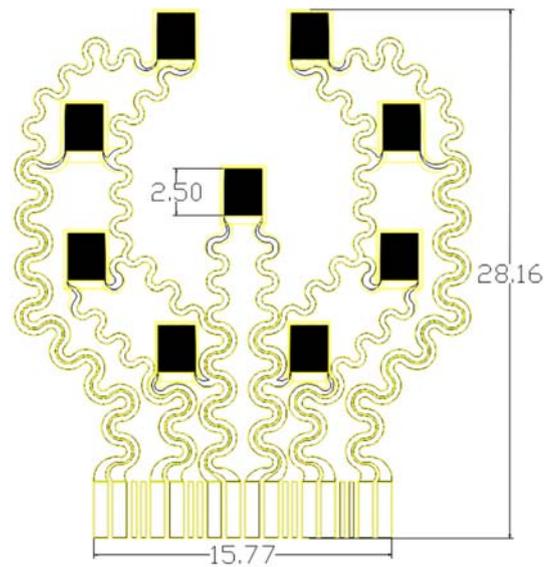
Figure 5.1: Array design. Dimensions in mm.
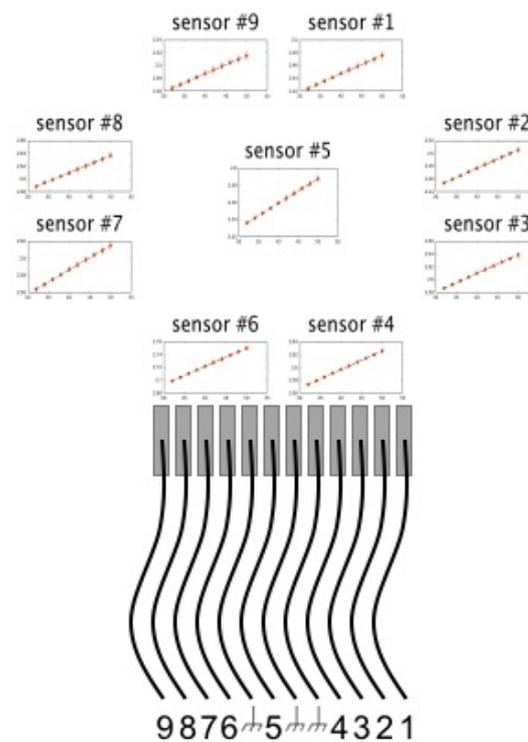
Figure 5.2: Sketch of wired device with sensors numeration. The boxes show calibration data.

Regarding the fabrication flow the process is exactly the same, but considering the dimensions that approx 60mm^2 the transfer process is more critical than the case of single sensor.

Due to the high number of sensor, the acquisition protocol has been modified from the previous case. Instead of using a high precision multimeter, as done for single sensor, an 12bit ADC (analog/digital converter) was used. A voltage divider has been design and assembled on a PCB to sense the voltages across each sensor and extract the temperatures of every spot of the array. The schematic of the acquisition set-up is shown in Fig. 5.3. A pulsed voltage has been provided to each sensor simultaneously and the voltage drop produced by each sensor was converted and saved into a database. Using the calibration data extracted for single sensor was possible to estimate the voltage variation due to temperature.

$$V_{sense} = V_{cc} \frac{R_{sense}}{R_{sense} + R_{fix}} \tag{5.1}$$

assuming the resistance in the voltage divider doesn't change with temperature and R_{sense} is the RTD, it gives:

$$
\begin{aligned}
\frac{dV}{dT} &= \frac{d}{dT}\left(V_{cc} \frac{R_{sense}}{R_{sense} + R_{fix}}\right) \\
&= Vcc \left(\frac{\frac{dR_{sense}}{dT}(R_{sense} + R_{fix}) - \frac{dR_{sense}}{dT} \, dR_{sense}}{(R_{sense} + R_{fix})^2}\right) \\
&= \frac{VccR_{fix}}{(R_{sense} + R_{fix})^2} \cdot \frac{dR_{sense}}{dT} \\
&= 2.91 \ mV/^{\circ}C
\end{aligned}
\tag{5.2}
$$

where $R_{sense} = 30\text{k}\Omega$ and $R_{fix} = 27\text{k}\Omega$ are used.
From the acquired voltage the related temperature has been extracted with:

$$T = T_0 + \frac{V - V_0}{k} \tag{5.3}$$

where T_0 and V_0 are temperature and voltage at an given known point and k is the voltage over temperature slope extracted from the calibration process Fig. 5.2.
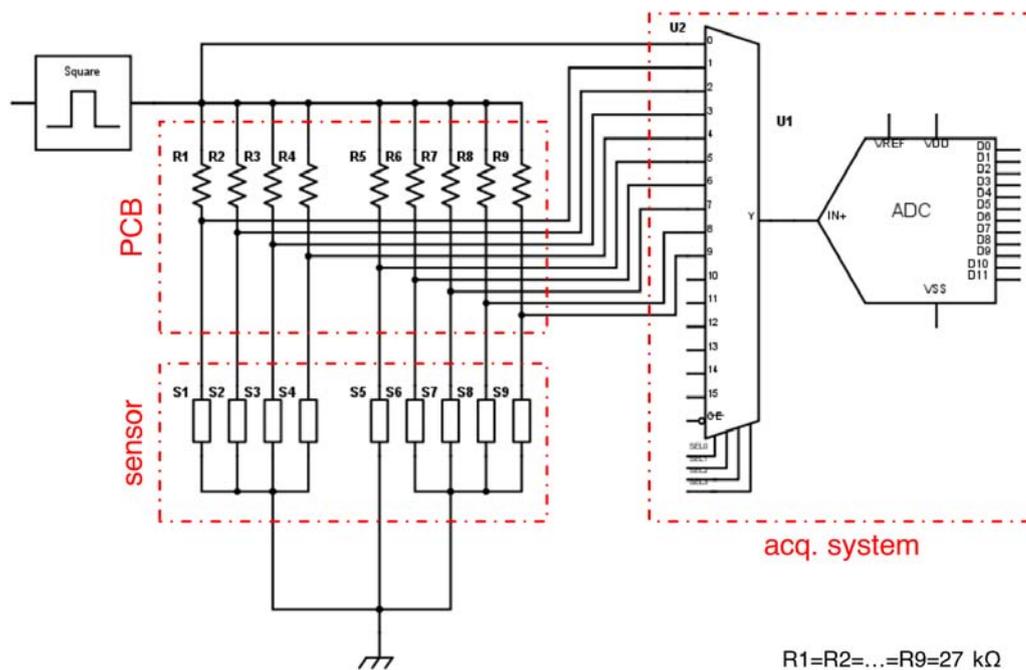
Figure 5.3: Acquisition setup scheme.
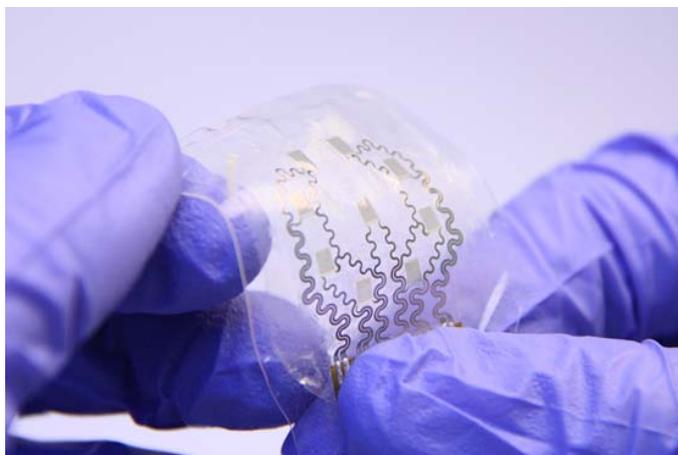
Figure 5.4: Array handled to show its transparency and bendable properties .

5.2 Proximity

As in case of the single sensor, the sensors array has been also tested for the detection the presence of hot objects in its proximity. In this case it has been use to map the heat distribution of a hand. In particular Fig. 5.5 shows the variation in temperature registered by the array when two fingers are placed ∼1 cm above the sensor. As the previous case (single sensor) a variation of 1 °C has been detected in the region where the fingers were placed, while a slighter increase occurred on the others sensors. This

shows the spatial resolution of the sensor even during contactless measurements.
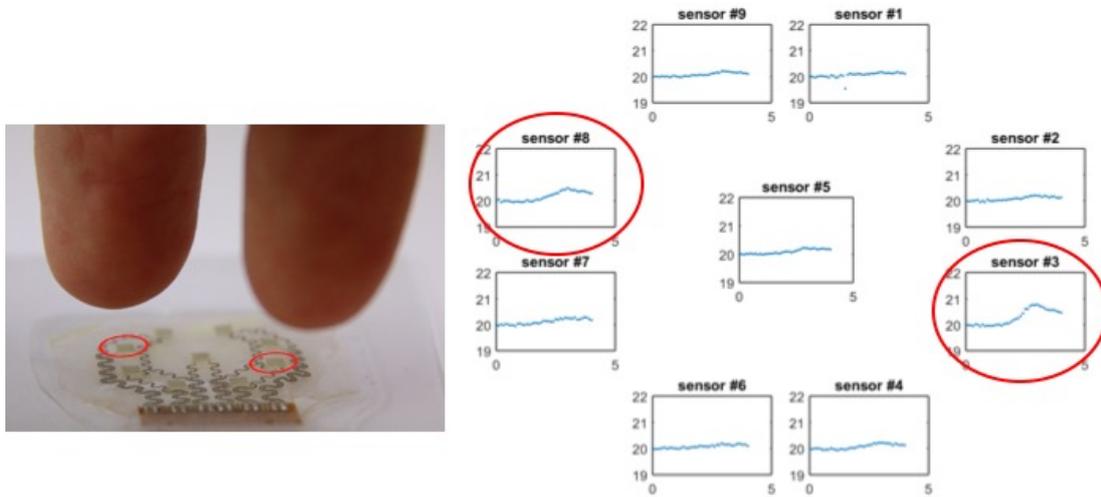
Figure 5.5: Mapping of heat distribution of human fingers placed 1 cm above the sensor.

5.3 Microfluidic

Another application of an array of temperature sensor is the mapping of flow.
To monitor the flow of a warm liquid a compostable fluidic device has been fabricated and integrated with the sensors array.

(a) Mold used for ecoflex casting

(b) Compostable device with channels for flow detection

Figure 5.6: Fabrication of microfluidic device.

The fabrication started from a teflon mold where some 3x1mm reliefs have been structured by milling (see Fig 5.6). Then some 30% ecoflex solution has been casted on top. After one night, when the solvent was completely evaporated, it was released from the mold and heat-sealed on top of a ~ 50um thick layer of 15% ecoflex deposited by spincoating. Finally a medical syringe needle was glued on one channel to allows the injection of the liquid. Then the sensor had been laying on top of the thin layer of ecoflex and connected to the acquisition system.
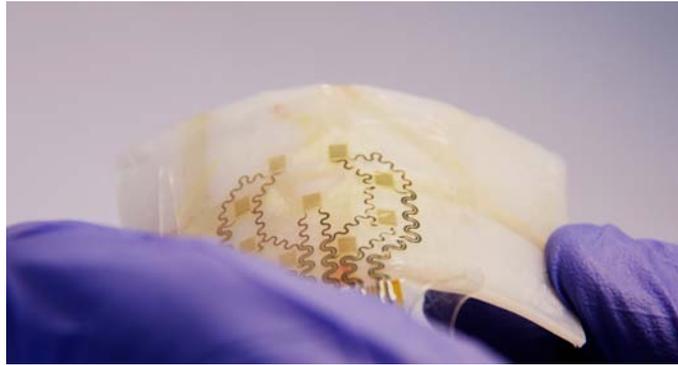
Figure 5.7: Sensor on bendable and compostable device for fluidic mapping.

To precisely and automatic control the exact amount of liquid injected a precise programmable syringe pump was used (see Fig. D.2). A 20mm medical syringe filled with red dyed water warmed up to 40°C was used to enhance its visibility.

Comparing thermal and standard pictures is clear the tremendous advance given by the sensor. In fact from standard pictures it's not clear which are che channel interested by water flow. This can only explained by IR cameras (expensive) or a matrix of temperature sensor. For example the upper channel is filled with some water but since it is cold is clear that it wasn't interested by water flow.
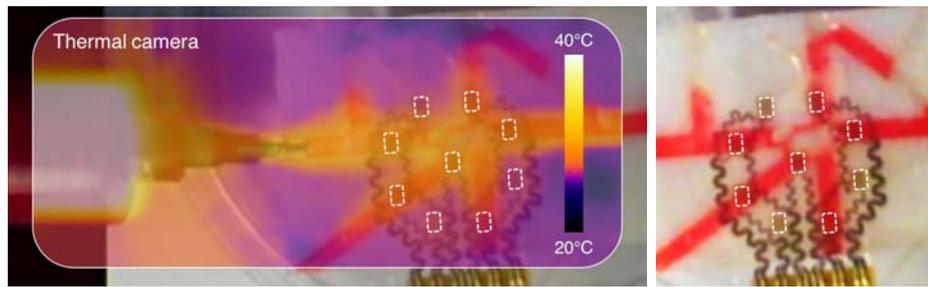
(a) Overlapping of optical and thermal and image

(b) Optical image of the setup
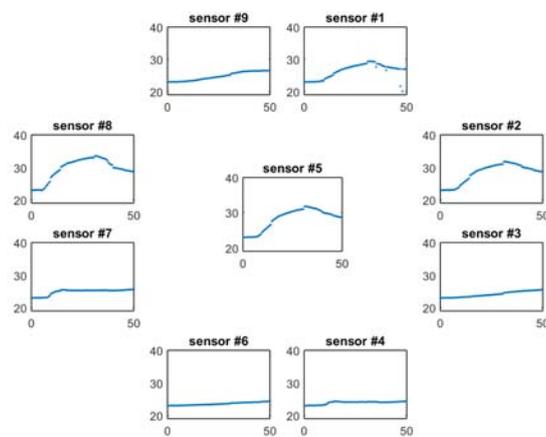
(c) Temperature sensed by the sensor

Figure 5.8: Flow mapping of warmed up dyed water.

Chapter 6

Dissolution

In this chapter, the results of the dissolution study are presented. The first part refers to the dissolution rates of pure Magnesium traces. Boh morphologichal and electrical characterization are studied. A comparison between two differents fluids is provided. Second the transient time of fully encapsulated is shown, which validate the basic concept of an encapsulation layer as an effective way to tune the degradation time

6.1 Dissolution of pure Mg

Although there is an extensive, existing body of knowledge related to corrosion of these metals in bulk form, far less information is available for thin films, where behaviors can be quite different [34].

The following outlines a study of dissolution behaviors, in terms of electrical, thickness, morphology and surface chemistry, of Mg thin films and serpentine wires in de-ionized (DI) water and in saline.

Fig. 6.1 summarizes representative dissolution behavior in terms of the change in resistance as a function of time for thin films of Mg in DI water and 150 mMol NaCl solutions both at RT. This concentration has been chosen to provided a simple simulation of body fluids for implantable devices. The geometry of the serpentine traces (width 10um; thickness 220nm; total length 20 mm) used for evaluations is the same as the single sensor (see Fig. 2.7 for design and 6.2 for optical changes).

Table 6.1: Dissolution rates of pure Mg obtained experimentally.

Material	Morphological dissolution rate [um/h]		Electrical dissolution rate [um/h]	
	DI water	saline	DI water	saline
pure Mg	0.11	0.47	1.32	3.3
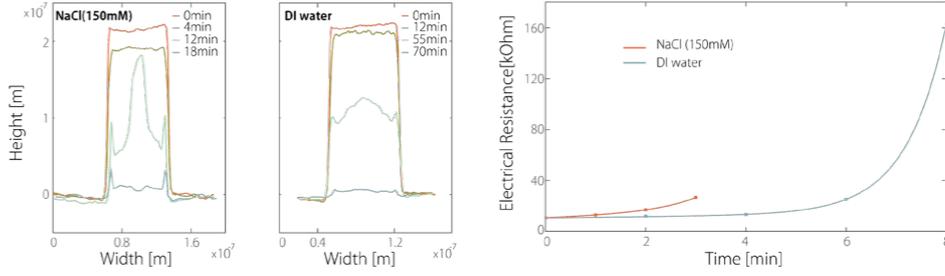
Figure 6.1: Dissolution behaviors of Mg traces. AFM and electrical measurements.

Changes in thickness with time for dissolution both in DI water and saline at RT appear in Fig. . In all cases, a silicon wafer covered with a thin layer of polyimide (PI) serves as substrate. A thin layer of Si_3N_4 (150nm) has been deposit between PI and Mg. This layer improves the yields and ensures that the dissolution kinetics are not interrupted by film delamination.

In order to compare the electrical and morphological dissolution rates a *electrical dissolution rates* (EDR) are defined by converting changes in electrical resistance to an effective (non-physical) thickness h (thickness equal to zero when R = ∞). Taking the initial height d_0 from the AFM (atomic force microscopy) measurement and the time passing by t_x into account, the electrical dissolution rate can be calculated as follow:

$$EDR = \frac{d_0}{t_x} \tag{6.1}$$

Results   The EDRs of Mg are higher for NaCl solution than DI water (2.5 times). This value raises to 4.3 if we consider the AFM measurements Table 6.1. In both cases this is likely due to the presence of chlorides (Cl^-) that promote rapid attack, as reported in corrosion studies of mass loss in bulk samples of Mg [35].

Because of its dissolution time in standard environmental conditions, elctronics only consisting of Mg would not be suitable for most applications.

To overcome this issue, the device should be encapsulated with layers that have a lower dissolution rate under the same conditions and so that the corrosion of Mg can be delayed.
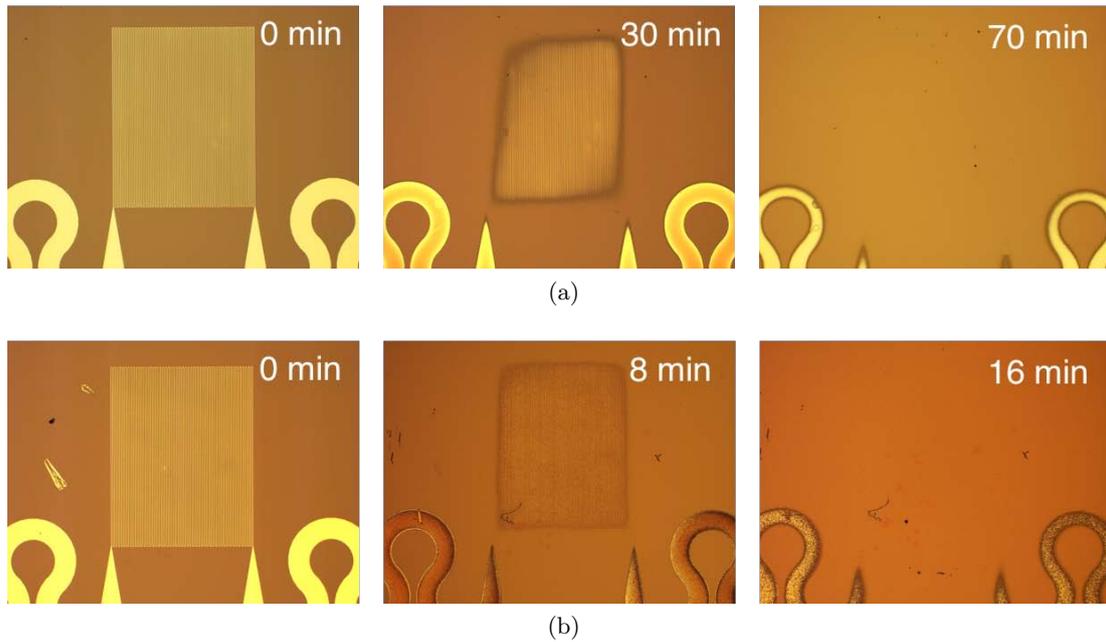
Figure 6.2: Optical changes of pure Mg on Silicon substrate during time. (a) DI water and (b) Saline.
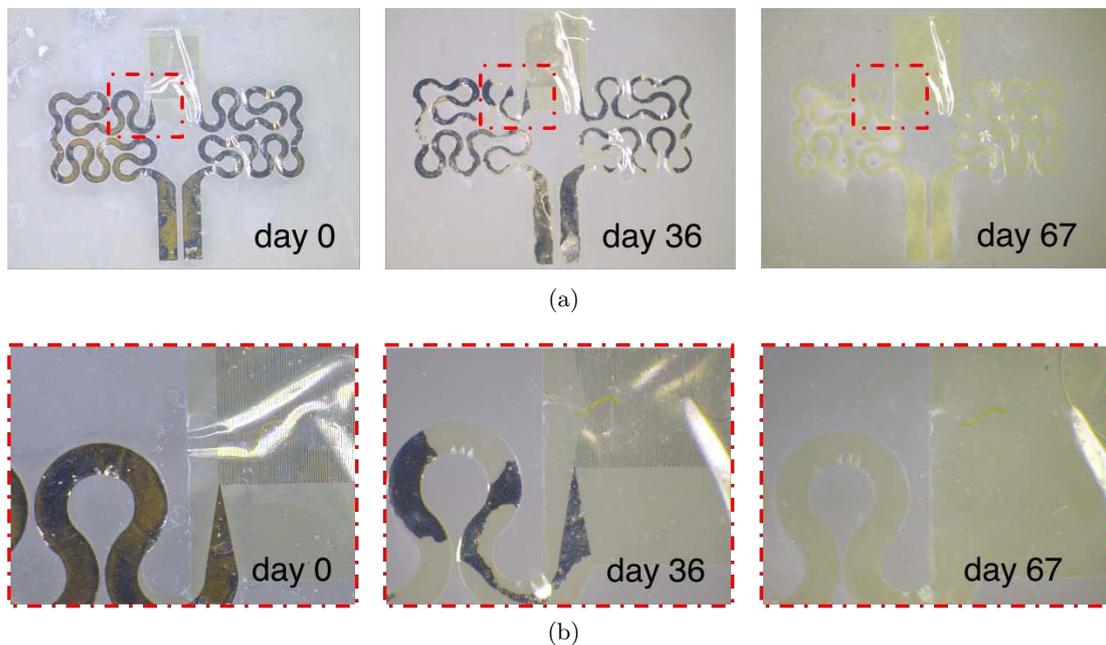
Figure 6.3: Morphological dissolution of fully encapsulated devices in NaCl 150mMol solution. (b) Particular between sensor and interconnection

6.2 Dissolution of final device

A summary of the dissolution of encapsulated devices is shown in Fig. 6.3. The dissolution of each encapsulated device in a 150mM saline solution was followed under

a light microscope for several days. The fully degradation of the devices occurred after about two months. The dissolution rates of the polymeric substrate and the encapsulating dielectric layers (SiO_2 and Si_3N_4) are assumed to be negligible over the timespan of the study. Therefore, mainly the morphological changes of Mg over time can be observed. Dissolution of Mg is essentially limited by the water and ion permeability of the polymer and dielectric layers. The small traces seem to be well protected by the encapsulation.

The attack of Mg occurred after several hours. This shows that the encapsulation with SiO_2, Si_3N_4 and ecoflex prolongs the lifetime of the device from some minutes to hours (the pure Mg circuit breaks after 4min in the same solution 6.1), stated by observing morphological changes.

For more precise statements regarding the full operation time of the device, a study determining the changes in resistance over time should be conducted.

Chapter 7

Conclusion and Outlook

In this chapter, a brief summary of the main results achieved during this work is given. To conclude, an outlook over the possible future work is presented.

7.1   Conclusion

This thesis, developed during the research at the ife (Institute for electronics) ETH Zürich show that transient temperature semsors are possible and they can be fabricated with very good performances. The main result achieved in this project can be resumed in several points listed in the following.

- A reliable fabrication protocol for thin film RTDs on soft substrate based on transfer printing has been defined

- Ecoflex, a biodegradable elastomer produced from starch and polylactic acid was used as substrate and encapsulation layer for our devices. It has been characterized from several point of view including optical mechanichal electrical and toxicity.

- High mechanical stability of the whole device were demonstrated. It was still perfectly working after folding/crumpling cycles. In addition it can be bended down to 1.75 mm radius and stretched in both direction up to 10%.

- The dissolution of the device was shown with two different approaches: pure Mg to test changes of electrical properties and long-term morphological study of encapsulated device to test transient time (67 days).

- Single-point measurement has been extended to mapping 9 points. It has been tested after the fabrication of a biodegradable and bendable fluidic device.

- Low thermal mass and small response time (5.9 ms) together high sensitivity (41 mK) complete the picture and show the dramatic potentiality of those devices.

7.2   Outlook

This work shows the high potentials of devices and materials. Additional tests can be done to explore other applications. Some further steps can include:

- The dissolution of the device. It should be further examined, especially in terms of changes in resistance over time, in order to fix the full operation time of the sensor before degradation process begins.

- Regarding ecoflex®, due to its softness and electrical properties it can be use as elastic dielectric for biodegradable pressure sensors or actuators. In addition its cytotoxicity should be in deeper inspected before its use in epidermal or implantable devices.

Our sensor can be integrated directly into food packaging. Many company have already started to use biodegradable polymers for that purpose. Providing the device with a wireless readout, food temperature can be tracked during the stocking time to ensure its freshness. This could pave the way to a new era in food packaging.

Bibliography

[1] Mihai Irimia-Vladu, Eric. D. Głowacki, Gundula Voss, Siegfried Bauer, and Niyazi Serdar Sariciftci. Green and biodegradable electronics. *Materials Today*, 15(7–8):340 – 346, 2012.

[2] Mihai Irimia-Vladu. "green" electronics: biodegradable and biocompatible materials and devices for sustainable future. *Chemical Society Reviews*, 43(2):588–610, 2014.

[3] Mihai Irimia-Vladu, Pavel A Troshin, Melanie Reisinger, Lyuba Shmygleva, Yasin Kanbur, Günther Schwabegger, Marius Bodea, Reinhard Schwödiauer, Alexander Mumyatov, Jeffrey W Fergus, et al. Biocompatible and biodegradable materials for organic field-effect transistors. *Advanced Functional Materials*, 20(23):4069–4076, 2010.

[4] S.W. Hwang, H. Tao, D.H. Him, H. Cheng, J.K. Song, E. Rill, M.A. Brenckle, B. Panailaitis, S.M. Won, Y.S. Kim, Y.M. SOng, K.J. Yu, A. Ameen, R. Li, Y. Su, M. Yang, D.L. Kaplan, M.R. Zakin, M.J. Slepian, Y. Huang, F.G. Omenetto, and J.A. Rogers. A physically transient form of silicon electronics. *Science*, 28, 2012.

[5] Canan Dagdeviren, Suk-Won Hwang, Yewang Su, Stanley Kim, Huanyu Cheng, Onur Gur, Ryan Haney, Fiorenzo G Omenetto, Yonggang Huang, and John A Rogers. Transient, biocompatible electronics and energy harvesters based on zno. *Small*, 9(20):3398–3404, 2013.

[6] Sung Hun Jin, Seung-Kyun Kang, In-Tak Cho, Sang Youn Han, Ha Uk Chung, Dong Joon Lee, Jongmin Shin, Geun Woo Baek, Tae-il Kim, Jong-Ho Lee, et al. Water-soluble thin film transistors and circuits based on amorphous indium–gallium–zinc oxide. *ACS applied materials & interfaces*, 7(15):8268–8274, 2015.

[7] D.H. Kim, Y.S. Kim, J. Amsden, B. Panilaitis, Kaplan. D.L., F.G. Omentetto, M.R. Zakin, and J.A. Rogers. Silicon electronics on silk as a path to bioresorbable, implantable devices. *Applied Physics Letters*, 95, 2009.

[8] C.J. Bettinger and Z. Bao. Organic thin-film transistors fabricated on resorbable biomaterial substrates. *Advanced Materials*, 22, 2010.

[9] Achim Walter, Wendy K Silk, and Ulrich Schurr. Environmental effects on spatial and temporal patterns of leaf and root growth. *Annual review of plant biology*, 60:279–304, 2009.

[10] R Chad Webb, Andrew P Bonifas, Alex Behnaz, Yihui Zhang, Ki Jun Yu, Huanyu Cheng, Mingxing Shi, Zuguang Bian, Zhuangjian Liu, Yun-Soung Kim, et al. Ultrathin conformal devices for precise and continuous thermal characterization of human skin. *Nature materials*, 12(10):938–944, 2013.

[11] Lan Yin, Huanyu Cheng, Shimin Mao, Richard Haasch, Yuhao Liu, Xu Xie, Suk-Won Hwang, Harshvardhan Jain, Seung-Kyun Kang, Yewang Su, Rui Li, Yonggang Huang, and John A. Rogers. Dissolvable metals for transient electronics. *Advanced Functional Materials*, 24(5):645–658, 2014.

[12] Dingchuan Xue, Yeoheung Yun, Zongqing Tan, Zhongyun Dong, and Mark J. Schulz. In vivo and in vitro degradation behavior of magnesium alloys as biomaterials. *Journal of Materials Science & Technology*, 28(3):261 – 267, 2012.

[13] Seung-Kyun Kang, Suk-Won Hwang, Huanyu Cheng, Sooyoun Yu, Bong Hoon Kim, Jae-Hwan Kim, Yonggang Huang, and John A. Rogers. Dissolution behaviors and applications of silicon oxides and nitrides in transient electronics. *Advanced Functional Materials*, 24(28):4427–4434, 2014.

[14] Kun Kelvin Fu, Zhengyang Wang, Jiaqi Dai, Marcus Carter, and Liangbing Hu. Transient electronics: Materials and devices. *Chemistry of Materials*, 28(11):3527–3539, 2016.

[15] S. BASF. ecoflex® f blend c1200 - product data sheet - basf plastics portal, `http://www.plasticsportal.net/wa/EU/Catalog/ePlastics/info/BASF/PRD/30516354`, [online; accessed 17.08.2016].

[16] Taghleef Industries. Product information - nativia ntss, bopla transparent film, both sides heat sealable, biodegradable, 2016.

[17] Innovia films, natureflex np datasheet. `http://www.innoviafilm.com/`.

[18] James E. Mark. Oxford University Press, 2009.

[19] P Kurzweil. Ac impedance spectroscopy—a powerful tool for the characterization of materials and electrochemical power sources. In *Proceedings of the 12-th International Seminar on Double Layer Capacitors and Similar Energy Storage Devices. Deerfield Beach: Florida (USA)*, volume 14, pages 18–32, 2004.

[20] Richard F. Wallin. A practical guide to iso 10993-5: Cytotoxicity. http://www.mddionline.com/article/practical-guide-iso-10993-5-cytotoxicity [Online accessed 14.08.16].

[21] Thomas Vasileiou, Daniele Foresti, Adem Bayram, Dimos Poulikakos, and Aldo Ferrari. Toward contactless biology: Acoustophoretic dna transfection. *Scientific Reports*, 6:20023 EP –, 02 2016.

[22] Resistance thermometer. `https://en.wikipedia.org/wiki/Resistance_thermometer`. [Online; accessed 19.08.2016].

[23] Jonathan A. Fan, Woon-Hong Yeo, Yewang Su, Yoshiaki Hattori, Woosik Lee, Sung-Young Jung, Yihui Zhang, Zhuangjian Liu, Huanyu Cheng, Leo Falgout, Mike Bajema, Todd Coleman, Dan Gregoire, Ryan J. Larsen, Yonggang Huang, and John A. Rogers. Fractal design concepts for stretchable electronics. *Nat Commun*, 5, 02 2014.

[24] A. Carlson, A.M. Bowen, Y. Huang, R.G. Nuzzo, and J.A. Rogers. Transfer printing techniques for materials assembly and micro/nanodevice fabrication. *Advanced Materials*, 24(39):5284–5318, 2012.

[25] Chi Hwan Lee, Dong Rip Kim, and Xiaolin Zheng. Fabricating nanowire devices on diverse substrates by simple transfer-printing methods. *Proceedings of the National Academy of Sciences*, 107(22):9950–9955, 2010.

[26] Tsuyoshi Sekitani, Shingo Iba, Yusaku Kato, Yoshiaki Noguchi, Takao Someya, and Takayasu Sakurai. Ultraflexible organic field-effect transistors embedded at a neutral strain position. *Applied Physics Letters*, 87(17), 2005.

[27] R. Renucci, L. Gaudart, J.P. Petrakian, and D. Roux. Electron transport properties of magnesium thin films. *Thin Solid Films*, 130:75–86, 1985.

[28] R Chad Webb, Yinji Ma, Siddharth Krishnan, Yuhang Li, Stephen Yoon, Xiaogang Guo, Xue Feng, Yan Shi, Miles Seidel, Nam Heon Cho, et al. Epidermal devices for noninvasive, precise, and continuous mapping of macrovascular and microvascular blood flow. *Science advances*, 1(9):e1500701, 2015.

[29] Heat capacities of the elements. `https://en.wikipedia.org/wiki/Heat_capacities_of_the_elements_(data_page)`. [Online; accessed 17.08.2016].

[30] Material property database - pecvd silicon oxide. `http://www.mit.edu/~6.777/matprops/sio2.htm`. [Online; accessed 17.08.2016].

[31] Material property database - pecvd silicon nitride. `http://www.mit.edu/~6.777/matprops/pecvd_sin.htm`. [Online; accessed 17.08.2016].

[32] Polylactic acid (pla, polylactide). `http://www.makeitfrom.com/material-properties/Polylactic-Acid-PLA-Polylactide/`. [Online; accessed 17.08.2016].

[33] Polymer property : Specific heat capacity. `http://www.lookpolymers.com/findproperty.php?pid=3&sx_id=875&value=1.88&type=1`. [Online; accessed 23.08.2016].

[34] John Wiley & Sons Inc Hobken NJ 2011. Uhlig's corrosion handbook. 3rd ed., (Ed. R. W. Revie).

[35] G. Song and A. Atrens. Understanding magnesium corrosion—a framework for improved alloy performance. *Advanced Engineering Materials*, 5(12):837–858, 2003.

Appendices

Appendix A

Fabrication steps in detail

Table A.1: List of all fabrication steps with description.

#	Step	Annotations
1	Clean wafer	Acetone/IPA/bakeout
		Or use new wafer
2	Sacrificial layer	PMMA 950K
		spin coat: 3000/3/30
		bake: 180°C for 1min
3	Mechanical support basis for fabrication	Polyimide HD4100
		spin coat: 1000/2/4, 5000/4/30
		bake: 90°C for 100s, 100°C for 100s
		cure: gradual heat up to 300°C, overnight
4	Bottom Encapsulation: Low-temperature silicon dioxide deposition	PECVD, 120°C, 100nm
5	Magnesium Layer	Sputtering, 250nm
		Litho, AZ1518
		spin coat: 3000/6/50, 5500/2/2
		bake: 115¡C for 120s
		expose: 50mJ
		develop: 10-15s in microposit
		Wet etching, HCl
		parameter: 10mmol/L for approx. 90s
6	Top Encapsulation: Low-temperature silicon nitride deposition	PECVD, 120°C, 100nm, with contact pads covered (Fig. A.1)
7	Second PI layer	120°C, 100nm, with contact pads covered
		Continued on next page

<div align="center">

Table A.1 – continued from previous page

</div>

#	Step	Annotations
		Polyimide HD4100
		spin coat: 1000/2/4, 5000/4/30
		bake: 90°C for 100s, 100°C for 100s
		cure: gradual heat up to 300°C, overnight
8	Patterning for Etching	PECVD, SiO_2, 120°C, 500nm
		Lithography, AZ4620
		spin coat: 3000/3/30
		bake: 110°C for 240s
		expose: 500mJ
		develop: 75s in 400K(dilution with DI water 1:3)
9	Dry Etching	RIE80
10	Release in Acetone (dissolution of sacrificial layer)	Wrap samples in wipe-covered glass slides and clamp it
		leave it in acetone overnight
		Put it out and let it dry for at least 1hr
11	Pickup on cellulose tape	
12	Backside PI dry etching (mechanical support layer)	RIE80 , 3+2min, 50W, PI etching program (alternatively RIE76)
13	Transfer on biodegradable ecoflex substrate	Substrate:
		Ecoflex, 15% w/v ecoflex in chlorophorm
		spin coat on a glass slide: 1500/5/60, repeat and let it dry at RT
		Transfer:
		Melt ecoflex on hotplate (135°C for 300s), stick samples with cellulose on top of ecoflex after 200s, then let it cool down and dissolve cellulose tape with DI water, dry
14	Top PI dry etching	RIE80, 5+4min, 50W, PI etching program (alternatively RIE76)
15	External wiring	solder wires
16	Encapsulation	Prepare top layer of ecoflex (same as step 13)
		Release from glass with a drop of DI water, dry
		Laminate on top of the structure
		Continued on next page

Table A.1 – continued from previous page

#	Step	Annotations
		Lets Ecoflex reflow on hotplate @135 C for 120s
17	Transfer and Encapsulation with gelatin solution	Optional
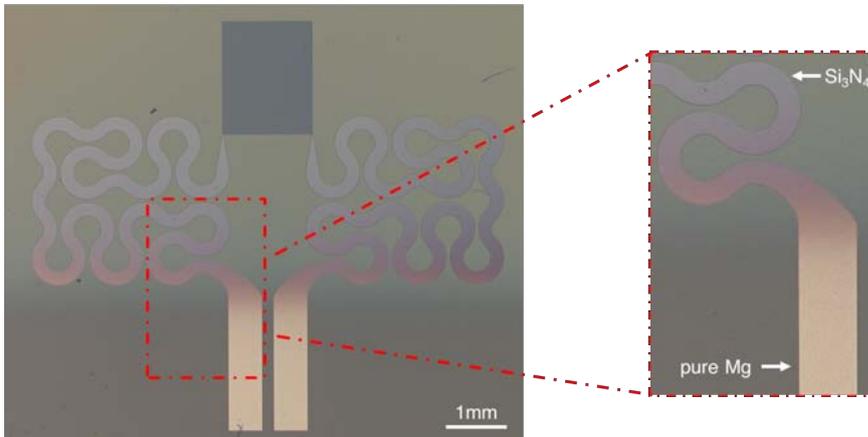
Figure A.1: Device after deposition of Si_2N_3 encapsulation layer. Pads where covered with glass slide to allow electrical contact.

Appendix B

Measurement protocol

To prevent systematic error from the equipment each point has been calculated as mean of 500 measurements by a high precision digital multimeter connected to a PC. To avoid self heating effect a square voltage with an amplitude of 5V and with a duration of 400us was applied, then the current flowing on the device was sampled in the middle of the pulse. Depending on the measurement the sampling time has been chosen: [0.1Hz] for long term monitoring; [1000Hz] To track fast changing in temperature (e.g. response time); [100Hz] All the others (e.g. bending, stretching ecc.)
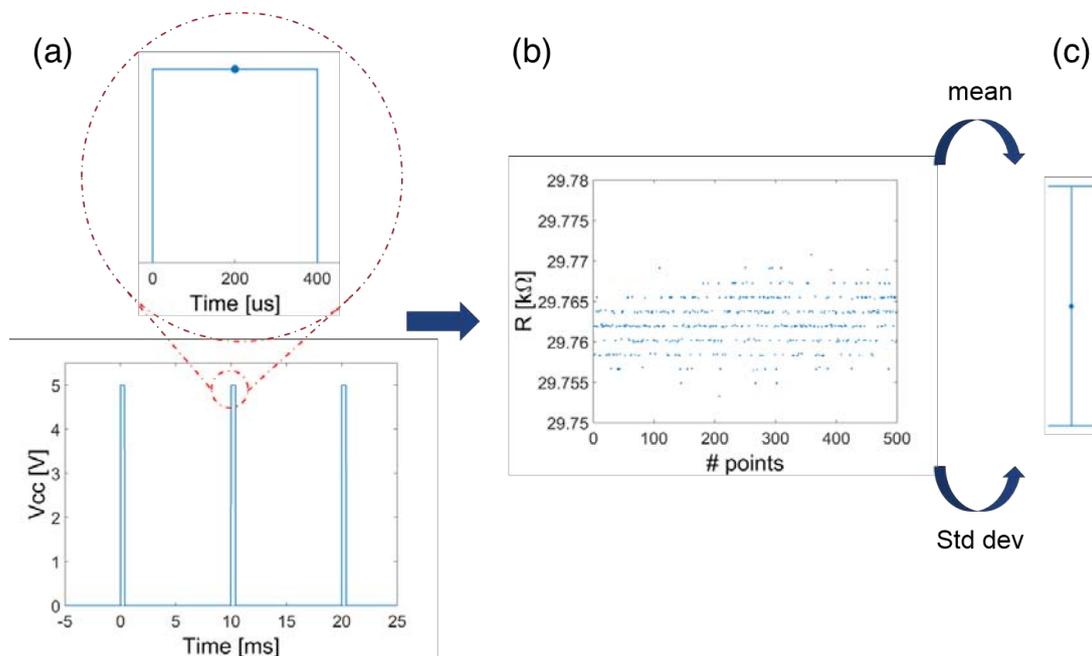
Figure B.1: Acquisition protocol developed for precise resistance measurement. (a)Signal applied to the resistor and sampling point. (b)Values collected after the measurement. (c)Mean and standard deviation calculation to derive the single entry in the plot

Appendix C

Capacitors
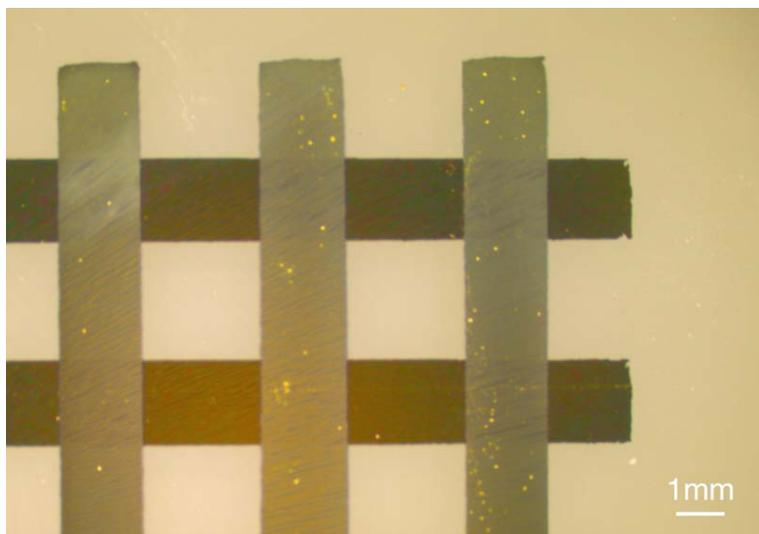
Figure C.1: Capacitors of the array.

C.1   Ecoflex® spincurve

In order to tune the desidered thickness the ecoflex spincurve has been performed. Several glass slide were coated with the same solution (5% w/v in Chloroform) at different speeds. After that, the thickness of each sample has been measured by profilometer four times in different spots. The averaged thickness for each speed are shown in Fig C.2
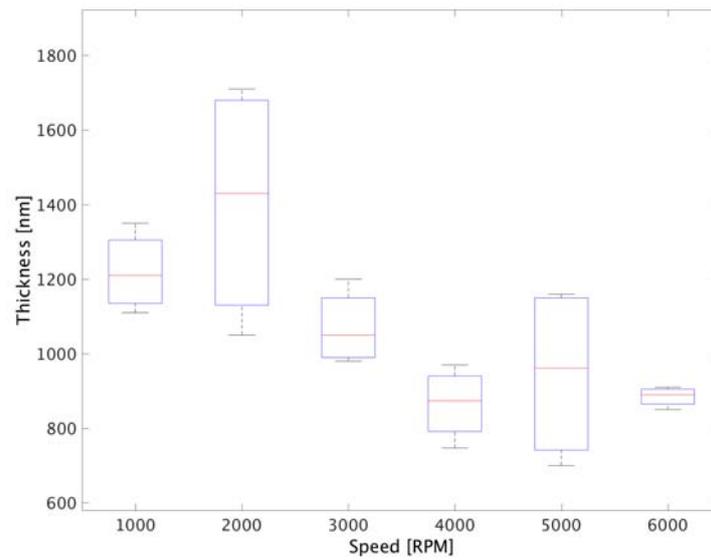
Figure C.2: Spincurve of 5% w/v ecoflex solution in chloroform.

C.2   Pressure sensor

Due to its softness ecoflex can be use not only as substrate but also as biodegradable dielectric for pressure sensor. Some tests have been made on the fabricated capacitors and the preliminary results are shown in the following.
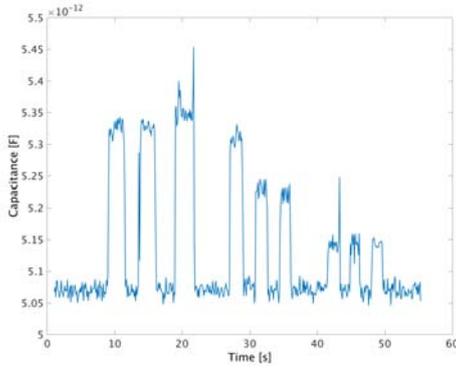
(a) Capacitance variation during time due to a different weight applied
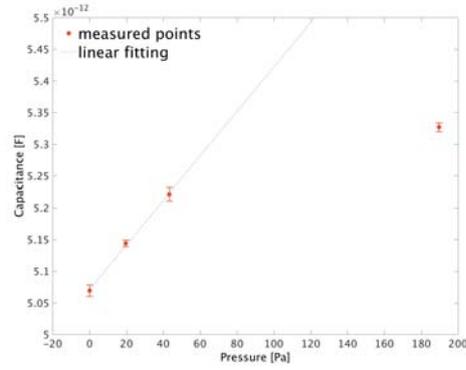
(b) Capacitance variation vs pressure
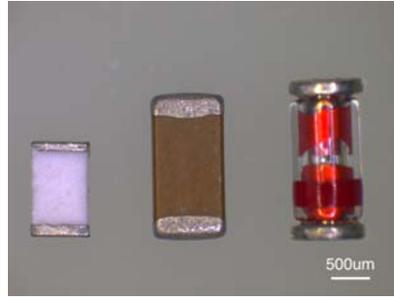
(c) Weights used

Figure C.3: Ecoflex explored as elastic dielectric for pressure sensor application.

A plate capacitor filled with a homogeneous dielectric has a capacitance

$$C = \varepsilon_0 \varepsilon_r \frac{A}{d} \tag{C.1}$$

Since we are interested in variation due to compression:

$$\frac{\delta C}{\delta d} = -\varepsilon_0 \varepsilon_r \frac{A}{d^2} \tag{C.2}$$

$$
\begin{aligned}
\Delta C &= -\varepsilon_0 \varepsilon_r \frac{A}{d^2} \cdot \Delta d \\
&= -\varepsilon_0 \varepsilon_r \frac{A}{d} \cdot \frac{\Delta d}{d}
\end{aligned} \tag{C.3}
$$

applying Hooke's Law

$$\Delta \sigma = -E \cdot \frac{\Delta d}{d} \tag{C.4}$$

where E is the Young modulus of the material and $\frac{\Delta d}{d}$ the fractional change in length

$$\Delta C = \varepsilon_0 \varepsilon_r \frac{A}{d} \cdot \frac{\Delta \sigma}{E} \qquad (C.5)$$

This means that theoretically the variation in capacitance over pressure is linear. In Fig. C.3a is reported the variation in capacitance over time while in Fig. C.3b are reported both theoretical and experimental data. The measured data well fit the theoretical for low pressure applied.

Appendix D

Setups and equipments

Figure D.1: Stretching setup used for testing.

Figure D.2: Setup used for liquid flow testing.